Generalization of Atmospheric Nonspherical Particle Size: Interconversions of Size Distributions and Optical Equivalence

Masanori Saito, Ping Yang

Department of Atmospheric Sciences, Texas A&M University, College Station, TX 77843

Corresponding author: Masanori Saito, masa.saito@tamu.edu

Early Online Release: This preliminary version has been accepted for publication in *Journal of the Atmospheric Sciences* cited, and has been assigned DOI 10.1175/JAS-D-22-0086.1. The final typeset copyedited article will replace the EOR at the above DOI when it is published.

ABSTRACT

Atmospheric particles exhibit various sizes and nonspherical shapes, which are factors that primarily determine the physical–optical properties of particles. The "sizes" of nonspherical particles can be specified based on various size descriptors, such as those defined with respect to a volume-equivalent spherical radius, projected-area-equivalent spherical radius, geometric radius, or effective radius. Microphysical and radiative transfer simulations as well as remote sensing implementations often require the conversions of particle size distributions (PSDs) in terms of the number concentration, projected area, and volume. The various size descriptors cause ambiguity in the PSD interconversion, and thereby result in potentially misleading quantification of the physical–optical properties of atmospheric nonspherical particles.

The present study aims to provide a generalized formula for interconversions of PSDs in terms of physical variables and size descriptors for arbitrary nonspherical particles with log-normal and gamma distributions. In contrast to previous studies, no empirical parameters are included, allowing intrinsic understanding of the nonspherical particle effects on the PSD interconversion. In addition, we investigate the impact of different size descriptors on the single-scattering properties of nonspherical particles. Consistent single-scattering properties among different nonspherical particles with the same size parameter are found when the size descriptor is the effective radius, whereby their mechanisms are suggested based on a modified anomalous diffraction theory.

The overarching goal of this work is to eliminate the ambiguity associated with a choice of the size descriptor of nonspherical particles for Earth-atmosphere system models, cloud–aerosol remote sensing, and analyses of *in-situ* measured atmospheric particles.

SIGNIFICANCE STATEMENT

Atmospheric dust and ice crystals have various sizes and mostly nonspherical shapes. Different definitions of these particle sizes and shapes causes uncertainties and even results in misleading solutions in the numerical modeling and remote sensing of atmospheric properties. We derived generalized analytical formulas to rigorously treat

the sizes and shapes of particles in the atmosphere, and also investigated the importance of the treatment of particle sizes on the particle properties essential to the Earth-atmospheric climate system. This study aims to eliminate the ambiguity associated with particle sizes and shapes in atmospheric research.

1. Introduction

Nonspherical particles, such as ice crystals, dust aerosols, and volcanic ash particles, are ubiquitous in the atmosphere, as confirmed by *in-situ* measurements (e.g., Volten et al., 2001; Reid et al., 2003a; Lawson et al., 2019; Magee et al., 2021). A single atmospheric particle exhibits various geometric characteristics such as particle habit or shape, aspect ratio, and microscopic irregularity or surface roughness (Kolorev and Issac, 2003; Um et al., 2015; Lindqvist et al., 2014). From a macroscopic view, these atmospheric particles are associated with a particle size distribution (PSD) that can span several orders of magnitude. These particle shape characteristics and PSDs are the critical factors in determining the physical (e.g., total volume and projected area of particles) and optical properties (e.g., the bulk extinction coefficient and phase matrix) of these atmospheric particles (Takano and Liou, 1989; Dubovik et al., 2006). Therefore, these characteristics must be realistically represented in atmospheric research applications such as Earth-atmosphere system models, cloud–aerosol remote sensing, and analyses of *in-situ* measured atmospheric particles.

Depending on the context, a preferred particle physical variable is chosen to depict the PSD of atmospheric particles, such as the number concentration dN/dr, the projected area distribution dA/dr, or the volume distribution dV/dr, where r is particle radius. The former two variables are essential to cloud-aerosol microphysics studies and radiative transfer computations, and the latter is often used for numerical model simulations of cloud and atmospheric aerosol fields. These PSDs are analytically convertible among the physical variables as derived by Hansen and Travis (1974) (hereinafter referred to as HT74) for spherical particles and have been widely used. However, PSD conversions for nonspherical particles involve uncertainties due to the ambiguity in defining the size of a nonspherical particle.

Accepted for publication in *Journal of the Atmospheric Sciences.* DOI 10.1175/JAS-D-22-0086.1.

Unlike a spherical particle, multiple particle sizes can be defined for an arbitrary nonspherical particle by using different size descriptors, such as the volume-equivalent spherical radius r_v, projected area-equivalent spherical radius r_a, geometric radius r_g, or effective radius of a single particle r_e. Petty and Huang (2011) (hereinafter referred to as PH11) elaborate on the analytical relationship of PSDs among various size descriptors for the modified gamma distribution of nonspherical particles. Ham et al. (2017) also discuss such analytical relations of PSDs for different nonspherical particles from the active-sensor remote sensing perspective. Although these previous studies have substantially elevated the level of understanding of nonspherical PSDs, the derived analytical relationships involve empirical parameters of nonspherical geometric characteristics, such as a coefficient in a volume–diameter relation that does not depict particle shapes explicitly. This hinders a more intuitive understanding of how the nonspherical geometric properties affect these analytical PSD interconversions.

From the optics perspective, a particle size is characterized with the size parameter kr, defined as 2π times the ratio of a particle "radius" r to the incident radiation wavelength λ, where $k = 2\pi/\lambda$. The use of different size descriptors to define the size parameters may cause ambiguity in the computed optical properties of atmospheric nonspherical particles for size parameters beyond the Rayleigh scattering regime. Previous studies have chosen a variety of size descriptors (Takano and Liou, 1989; Chylék and Videen, 1994; Yang et al., 2013), which have made it difficult to perform a straightforward comparison of the single-scattering properties of nonspherical particles using different size descriptors. The effective radius r_e was suggested by Grenfell and Warren (1999) (hereinafter referred to as GW99) as an optimal choice of the size descriptor for a nonspherical particle, but the theoretical rationale behind this approach has not yet been clarified. Therefore, it is essential to bridge the gap in understanding the potential impacts of a choice of the size descriptor on the optical property simulations involving nonspherical particles.

This work is inspired by the previous studies (HT74, GW99, and PH11) and is aimed to fill the remaining gap in the understanding of the impacts of a choice of the size descriptor on the physical and optical properties of arbitrary atmospheric nonspherical particles without ambiguity. In particular, the analytical formulation in this paper will not use empirical parameters but physically rational parameters related to the nonspherical geometric characteristics. Important definitions of particle sizes and shapes are described in Section 2. Section 3 briefly reviews the concept of PSD and its interconversion for spherical particles. Analytical formulas for the PSD interconversions of nonspherical particles are derived in Section 4. Section 5 discusses the impacts of a choice of the size descriptor on the optical properties of nonspherical particles. Section 6 summarizes and discusses the significance of our findings in atmospheric science applications.

2. Size and Shape Definitions

a. Size descriptors for nonspherical particles

As mentioned above, the four primary types of the size descriptor of a single nonspherical particle are volume-equivalent spherical radius r_v, projected area-equivalent spherical radius r_a, geometric radius r_g, and effective radius r_e. Here we do not discuss other potential size descriptors including particle mass (Petty and Huang, 2010) or aerodynamic size (Hinds, 1999).

For a single particle with volume v and average projected area a under the random orientation condition, these four particle size descriptors are

$$r_\mathrm{v} = \left(\frac{3v}{4\pi}\right)^{\frac{1}{3}}, \tag{1}$$

$$r_\mathrm{a} = \left(\frac{a}{\pi}\right)^{\frac{1}{2}}, \tag{2}$$

$$r_\mathrm{e} = \frac{3v}{4a}, \tag{3}$$

$$r_\mathrm{g} = (\text{half of the maximum length of a particle}), \tag{4}$$

where the maximum length of a particle is either the diameter of the smallest circumscribed sphere of an irregularly shaped particle (e.g., Saito et al., 2021) or the maximum dimension of a regular nonspherical particle (e.g., Yang et al., 2013). For simplicity, we define r_g as the radius of the smallest circumscribed sphere of a particle throughout this paper.

b. Shape descriptors for nonspherical particles

Accepted for publication in *Journal of the Atmospheric Sciences.* DOI 10.1175/JAS-D-22-0086.1.

The present definition of the macroscopic particle shape is based on the geometric characteristics that primarily determine the v and a of a particle. The degree of sphericity Ψ is a dimensionless parameter describing the resemblance of the particle shape to a sphere. It is determined by v and the surface area s of a particle (Wadell, 1935). However, for complex concave particles, s cannot be easily quantified. Saito and Yang (2021) defined the degree of effective sphericity through expanding Ψ by substituting $s = 4a$ based on the random orientation assumption for a convex particle (Vouk, 1948) as

$$\Psi_\mathrm{e} = \frac{\pi^{\frac{1}{3}}(6v)^{\frac{2}{3}}}{4a}, \tag{5}$$

where it satisfies $\Psi_\mathrm{e} = \Psi$ for convex particles. For simplicity, we omit subscript e in the following text, and therefore Ψ should be regarded as the degree of effective sphericity.

Other parameters that describe the geometric properties of nonspherical particles are the volume ratio V_r and area ratio A_r (Heymsfield and Miloshevich, 2003) relative to those of the smallest circumscribed sphere of a particle and the smallest circle of an average projected particle, respectively, as follows:

$$V_\mathrm{r} = \frac{3v}{4\pi r_\mathrm{g}^3}, \tag{6}$$

$$A_\mathrm{r} = \frac{a}{\pi r_\mathrm{g}^2}, \tag{7}$$

where Eq. (6) is often multiplied by the solid ice density and used as the effective ice density (Heymsfield et al., 2004).

c. Theoretical relationship among size descriptors

A dimensionless coefficient can convert a particle size among the four size descriptors for nonspherical particles. From Eqs. (1–7), the conversion of the particle size from one size descriptor p to another q for an arbitrary nonspherical particle is obtained through

$$q = \alpha_\mathrm{pq} p, \tag{8}$$

where a set of coefficients α_pq for all conversions is tabulated in Table 1.

Table 1. Coefficients α for the conversion of a particle size from one size descriptor (column heading) to another (row heading) in Eq. (8), and physical variables (volume v and projected area a) of a particle expressed with various size descriptors.

Conversion to	Conversion from			
	r_{v}	r_{a}	r_{g}	r_{e}
r_{v}	1	$\Psi^{\frac{1}{2}}$	$\Psi^{-1}\left(\frac{V_{\mathrm{r}}}{A_{\mathrm{r}}}\right)$	Ψ^{-1}
r_{a}	$\Psi^{-\frac{1}{2}}$	1	$\Psi^{-\frac{3}{2}}\left(\frac{V_{\mathrm{r}}}{A_{\mathrm{r}}}\right)$	$\Psi^{-\frac{3}{2}}$
r_{g}	$\Psi\left(\frac{V_{\mathrm{r}}}{A_{\mathrm{r}}}\right)^{-1}$	$\Psi^{\frac{3}{2}}\left(\frac{V_{\mathrm{r}}}{A_{\mathrm{r}}}\right)^{-1}$	1	$\left(\frac{V_{\mathrm{r}}}{A_{\mathrm{r}}}\right)^{-1}$
r_{e}	Ψ	$\Psi^{\frac{3}{2}}$	$\left(\frac{V_{\mathrm{r}}}{A_{\mathrm{r}}}\right)$	1
v	$\frac{4}{3}\pi r_{\mathrm{v}}^3$	$\frac{4}{3}\pi\Psi^{\frac{3}{2}}r_{\mathrm{a}}^3$	$\frac{4}{3}\pi V_{\mathrm{r}} r_{\mathrm{g}}^3$	$\frac{4}{3}\pi\Psi^{-3}r_{\mathrm{e}}^3$
a	$\pi\Psi^{-1}r_{\mathrm{v}}^2$	πr_{a}^2	$\pi A_{\mathrm{r}} r_{\mathrm{g}}^2$	$\pi\Psi^{-3}r_{\mathrm{e}}^2$

The coefficients are mainly described by Ψ, which ranges from $0 < \Psi < 1$ for nonspherical particles. From Table 1 and the definition of r_{g}, the size descriptors satisfy a relation of $r_{\mathrm{e}} < r_{\mathrm{v}} < r_{\mathrm{a}} < r_{\mathrm{g}}$, because $\Psi^c < 1$ for any $c > 0$ and vice versa. In addition, the analytical expressions of v and a for a nonspherical particle described with each size descriptor are similar to those for a sphere, but multiplied by a coefficient including Ψ, V_{r}, or A_{r}.

3. A Brief Review of Size Distributions

a. General properties of size distributions

A PSD is defined as the total amount of a physical variable x of particles per unit volume of the air $\frac{dx(p)}{dp}dp$ whose size p falls within an infinitesimal range of particle size $[p, p + dp]$ (e.g., PH11). The particle size bin intervals can be logarithmic $[\ln p\,, \ln p + d\ln p]$. The physical variable of particles can be the number, projected area, or volume concentration. Also, the particle size can be defined by particle radius, diameter, or anything that gives a unique size-descriptive quantity.

PSDs in terms of the number, projected area, and volume concentrations with linear or logarithmic size intervals are interconvertible from the fact that $d\ln p = \frac{1}{p}dp$, described (e.g., Dubovik et al., 2006) as

$$\frac{dN(p)}{dp} = \frac{1}{p}\frac{dN(p)}{d\ln p}, \tag{9}$$

$$\frac{dA(p)}{dp} = \frac{1}{p}\frac{dA(p)}{d\ln p} = a(p)\frac{dN(p)}{dp}, \tag{10}$$

$$\frac{dV(p)}{dp} = \frac{1}{p}\frac{dV(p)}{d\ln p} = v(p)\frac{dN(p)}{dp}. \tag{11}$$

The integrated physical quantities over a PSD are described as follows:

$$N_{\mathrm{T}} = \int_0^\infty \frac{dN(p)}{dp}dp, \tag{12}$$

$$A_{\mathrm{T}} = \int_0^\infty a(p)\frac{dN(p)}{dp}dp, \tag{13}$$

$$V_{\mathrm{T}} = \int_0^\infty v(p)\frac{dN(p)}{dp}dp, \tag{14}$$

$$M_i = \int_0^\infty p^i\frac{dN(p)}{dp}dp, \tag{15}$$

where N_{T}, A_{T}, and V_{T} are the total number, total projected area, and total volume concentration, respectively; and M_i is the i-th moment of a given PSD in terms of the number concentration.

b. Common size distributions for spherical particles

A PSD formula for spherical particles originated from HT74, which was motivated to minimize the number of governing parameters of PSD to facilitate inversions of scattering measurements. One of the two essential PSD parameters is the effective radius $\langle R_{\mathrm{eff}}\rangle$ (angle brackets are used to avoid confusion with the effective radius of a single particle r_{e}), defined as a particle radius weighted with the particle projected area over a PSD, because the amount of the scattered light by a particle is nearly proportional to the projected area of a particle for size parameters far beyond the Rayleigh scattering regime (e.g., $kr > 5$). If r is the radius of a sphere, then $\langle R_{\mathrm{eff}}\rangle$ is described as (HT74):

$$\langle R_{\mathrm{eff}}\rangle = \frac{\int_0^\infty r\pi r^2\frac{dN(r)}{dr}dr}{\int_0^\infty \pi r^2\frac{dN(r)}{dr}dr} = \frac{\int_0^\infty r^3\frac{dN(r)}{dr}dr}{\int_0^\infty r^2\frac{dN(r)}{dr}dr} = \frac{M_3}{M_2}, \tag{16}$$

which can also be expressed as the ratio of the third moment to the second moment of a dN/dr for spherical particles. Similarly, the effective variance of a PSD $\langle V_{\mathrm{eff}}\rangle$, a dimensionless parameter as a measure of a PSD width, is defined as

Accepted for publication in *Journal of the Atmospheric Sciences.* DOI 10.1175/JAS-D-22-0086.1.

$$\langle V_{\mathrm{eff}} \rangle = \frac{\int_0^\infty (r - \langle R_{\mathrm{eff}} \rangle)^2 \pi r^2 \frac{dN(r)}{dr} dr}{\langle R_{\mathrm{eff}} \rangle^2 \int_0^\infty \pi r^2 \frac{dN(r)}{dr} dr}. \tag{17}$$

Among various PSDs proposed and used for atmospheric science applications, the log-normal distribution (LND) and the gamma distribution (GD) are the two major PSDs used for aerosol (e.g., Nakajima et al., 1996) and ice clouds (e.g., Heymsfield et al., 2013), respectively.

1) LOG-NORMAL DISTRIBUTION

The analytical PSD expression in terms of the LND number concentration is described as

$$\frac{dN(r)}{dr} = \frac{1}{r} \frac{N_{\mathrm{T}}}{\ln S \sqrt{2\pi}} \exp\left[-\frac{1}{2}\left(\frac{\ln r - \ln \hat{r}_{\mathrm{N}}}{\ln S}\right)^2\right], \tag{18}$$

where $\hat{r}_{\mathrm{x}}$ and S are the median particle radius and geometric standard deviation of the PSD in terms of a physical variable of particles x, respectively. The i-th moment of the log-normal PSD in terms of the number concentration is given by

$$M_i = \hat{r}_{\mathrm{N}}^i \exp\left[\frac{i^2}{2} \ln^2 S\right]. \tag{19}$$

From Eqs. (10–11, 18–19), the log-normal PSDs in terms of the projected area and volume concentrations are written as

$$\frac{dA(r)}{dr} = \frac{1}{r} \frac{A_{\mathrm{T}}}{\ln S \sqrt{2\pi}} \exp\left[-\frac{1}{2}\left(\frac{\ln r - \ln \hat{r}_{\mathrm{A}}}{\ln S}\right)^2\right], \tag{20}$$

$$\frac{dV(r)}{dr} = \frac{1}{r} \frac{V_{\mathrm{T}}}{\ln S \sqrt{2\pi}} \exp\left[-\frac{1}{2}\left(\frac{\ln r - \ln \hat{r}_{\mathrm{V}}}{\ln S}\right)^2\right], \tag{21}$$

where

$$A_{\mathrm{T}} = \pi \hat{r}_{\mathrm{N}}^2 N_{\mathrm{T}} \exp[2 \ln^2 S], \tag{22}$$

$$V_{\mathrm{T}} = \frac{4}{3} \pi \hat{r}_{\mathrm{N}}^3 N_{\mathrm{T}} \exp\left[\frac{9}{2} \ln^2 S\right], \tag{23}$$

$$\hat{r}_{\mathrm{A}} = \hat{r}_{\mathrm{N}} \exp[2 \ln^2 S], \tag{24}$$

$$\hat{r}_{\mathrm{V}} = \hat{r}_{\mathrm{N}} \exp[3 \ln^2 S], \tag{25}$$

and S is invariant through these conversions. The effective radius and variance for the log-normal PSD are derived by substituting Eq. (18) into Eqs. (16–17) as

$$\langle R_{\mathrm{eff}} \rangle = \hat{r}_{\mathrm{N}} \exp\left[\frac{5}{2} \ln^2 S\right], \tag{26}$$

$$\langle V_{\mathrm{eff}} \rangle = \exp[\ln^2 S] - 1. \tag{27}$$

As a similar analog of LND, a multimodal LND (e.g., Ahmad et al., 2010) can be described with a superimposed set of multiple LNDs through defining ratios of the physical variables among each mode of a PSD.

2) GAMMA DISTRIBUTION

Similarly, the gamma PSD in terms of the number concentration is described as

$$\frac{dN(r)}{dr} = \frac{N_{\mathrm{T}}\Lambda^{\mu_{\mathrm{N}}}}{\Gamma(\mu_{\mathrm{N}})} r^{\mu_{\mathrm{N}}-1} \exp[-\Lambda r], \tag{28}$$

where $\Gamma(\mu_{\mathrm{x}})$ is the complete gamma function; Λ and μ_{x} are the slope and dispersion parameters of the PSD in terms of a physical variable of particles x, respectively. The i-th moment of the gamma PSD in terms of the number concentration is

$$M_i = \frac{N_{\mathrm{T}}\Lambda^{-i}}{\mu_{\mathrm{N}}} \prod_{j=0}^{i} (\mu_{\mathrm{N}} + j). \tag{29}$$

The gamma PSDs in terms of the projected area and volume concentrations are derived from Eqs. (10–11, 28–29) as

$$\frac{dA(r)}{dr} = \frac{A_{\mathrm{T}}\Lambda^{\mu_{\mathrm{A}}}}{\Gamma(\mu_{\mathrm{A}})} r^{\mu_{\mathrm{A}}-1} \exp[-\Lambda r], \tag{30}$$

$$\frac{dV(r)}{dr} = \frac{V_{\mathrm{T}}\Lambda^{\mu_{\mathrm{V}}}}{\Gamma(\mu_{\mathrm{V}})} r^{\mu_{\mathrm{V}}-1} \exp[-\Lambda r], \tag{31}$$

where

$$A_{\mathrm{T}} = \pi\Lambda^{-2} N_{\mathrm{T}} \prod_{i=0}^{1} (\mu_{\mathrm{N}} + i), \tag{32}$$

$$V_{\mathrm{T}} = \frac{4\pi}{3}\Lambda^{-3} N_{\mathrm{T}} \prod_{i=0}^{2} (\mu_{\mathrm{N}} + i), \tag{33}$$

$$\mu_{\mathrm{A}} = \mu_{\mathrm{N}} + 2, \tag{34}$$

$$\mu_{\mathrm{V}} = \mu_{\mathrm{N}} + 3, \tag{35}$$

and Λ is unchanged through these conversions. The effective radius and variance for the gamma PSD are

$$\langle R_{\mathrm{eff}} \rangle = \frac{\mu_{\mathrm{N}}+2}{\Lambda}, \tag{36}$$

$$\langle V_{\mathrm{eff}} \rangle = \frac{1}{\mu_{\mathrm{N}}+2}. \tag{37}$$

According to HT74, Eq. (28) can be rewritten as

$$\frac{dN(r)}{dr} = N_0 r^{\frac{1-3\langle V_{\mathrm{eff}} \rangle}{\langle V_{\mathrm{eff}} \rangle}} \exp\left[-\frac{1}{\langle R_{\mathrm{eff}} \rangle \langle V_{\mathrm{eff}} \rangle} r\right], \tag{38}$$

where an intercept N_0 is

Accepted for publication in *Journal of the Atmospheric Sciences.* DOI 10.1175/JAS-D-22-0086.1.

$$N_0 = \frac{N_{\mathrm{T}}\left(\frac{1}{\langle R_{\mathrm{eff}}\rangle\langle V_{\mathrm{eff}}\rangle}\right)^{\frac{1-2\langle V_{\mathrm{eff}}\rangle}{\langle V_{\mathrm{eff}}\rangle}}}{\Gamma\left(\frac{1-2\langle V_{\mathrm{eff}}\rangle}{\langle V_{\mathrm{eff}}\rangle}\right)}. \tag{39}$$

A particular case of GD includes a power-law distribution (e.g., Junge, 1955) useful for aerosol PSD by applying $\Lambda = 0$ to Eq. (28). Note that the moment of a power-law distribution and GD with $\mu_{\mathrm{N}} \leq 0$ can be obtained by specifying a finite particle size range (e.g., PH11).

4. Theoretical Conversions of Size Distributions

Let a PSD be rewritten as a generalized form $\frac{dx(p)}{dp}$, where $x(p)$ is a physical variable (i.e., N, A, or V) of arbitrary nonspherical particles expressed with a particle size descriptor p (i.e., r_{v}, r_{a}, r_{g}, or r_{e}). To simplify the problem, here we begin with a theoretical derivation of the PSD interconversions in the case of a size-invariant particle shape that is a common assumption for cloud–aerosol remote sensing applications (e.g., Platnick et al., 2016; Lee et al., 2017). We consider a conversion of a PSD from $\frac{dx(p)}{dp}$ into $\frac{dy(q)}{dq}$ in terms of another physical variable of particles y expressed with another particle size descriptor q. As physical variables of particles and size descriptors are interconvertible (Eqs. 8–14 and Table 1), we let these variables be $x(y)$ and $p(q)$. The conversions of PSDs can be achieved by solving

$$\frac{dy(q)}{dq} = \frac{dx_p\{y_p[p(q)]\}}{dp}\frac{dy_p}{dx_p}\frac{dp}{dq}, \tag{40}$$

where $\frac{dy_p}{dx_p}$ is a derivative of a physical variable with respect to another physical variable expressed with size descriptor p, and $\frac{dp}{dq}$ is a derivative of a referenced size descriptor with respect to another.

a. Log-normal distributions

Solving Eq. (40) in conjunction with log-normal PSDs, we have

$$\frac{dy(q)}{dq} = \frac{1}{q}\frac{y_{\mathrm{T,q}}}{\ln S\sqrt{2\pi}}\exp\left[-\frac{1}{2}\left(\frac{\ln q - \ln \hat{q}_{\mathrm{y}}}{\ln S}\right)^2\right], \tag{41}$$

where new parameters $y_{\mathrm{T,q}}$ and $\hat{q}_{\mathrm{y}}$ are expressed with a set of old parameters $x_{\mathrm{T,p}}$ and $\hat{p}_{\mathrm{x}}$. A complete set of the parameters for PSD conversions among physical variables (N, A, and V) and size descriptors (r_{v}, r_{a}, r_{g}, and r_{e}) is tabulated in Table 2.

Table 2. A complete set of the coefficients for interconversions of log-normal PSDs from one (column heading) to another (row heading) in Eq. (41).

Parameters in the target LND		Parameters in the source LND		
		$\frac{dN}{dp}$	$\frac{dA}{dp}$	$\frac{dV}{dp}$
		$N_{\mathrm{T,p}}$	$A_{\mathrm{T,p}}$	$V_{\mathrm{T,p}}$
$\frac{dN}{dq}$	$N_{\mathrm{T,q}}$	$N_{\mathrm{T,p}}$	$\pi\hat{p}_{\mathrm{A}}^{-2}\alpha_{\mathrm{pa}}^{-2}A_{\mathrm{T,p}}\exp\left[2\ln^2 S\right]$	$\frac{3}{4\pi}\hat{p}_{\mathrm{V}}^{-3}\alpha_{\mathrm{pv}}^{-3}V_{\mathrm{T,p}}\exp\left[\frac{9}{2}\ln^2 S\right]$
$\frac{dA}{dq}$	$A_{\mathrm{T,q}}$	$\pi\hat{p}_{\mathrm{N}}^{2}\alpha_{\mathrm{pa}}^{2}N_{\mathrm{T,p}}\exp\left[2\ln^2 S\right]$	$A_{\mathrm{T,p}}$	$\frac{3}{4}\hat{p}_{\mathrm{V}}^{-1}\alpha_{\mathrm{pe}}^{-1}V_{\mathrm{T,p}}\exp\left[\frac{1}{2}\ln^2 S\right]$
$\frac{dV}{dq}$	$V_{\mathrm{T,q}}$	$\frac{4}{3}\pi\hat{p}_{\mathrm{N}}^{3}\alpha_{\mathrm{pv}}^{3}N_{\mathrm{T,p}}\exp\left[\frac{9}{2}\ln^2 S\right]$	$\frac{4}{3}\hat{p}_{\mathrm{A}}\alpha_{\mathrm{pe}}A_{\mathrm{T,p}}\exp\left[\frac{1}{2}\ln^2 S\right]$	$V_{\mathrm{T,p}}$
		$\hat{p}_{\mathrm{N}}$	$\hat{p}_{\mathrm{A}}$	$\hat{p}_{\mathrm{V}}$
$\frac{dN}{dq}$	$\hat{q}_{\mathrm{N}}$	$\alpha_{\mathrm{pq}}\hat{p}_{\mathrm{N}}$	$\alpha_{\mathrm{pq}}\hat{p}_{\mathrm{A}}\exp\left[-2\ln^2 S\right]$	$\alpha_{\mathrm{pq}}\hat{p}_{\mathrm{V}}\exp\left[-3\ln^2 S\right]$
$\frac{dA}{dq}$	$\hat{q}_{\mathrm{A}}$	$\alpha_{\mathrm{pq}}\hat{p}_{\mathrm{N}}\exp\left[2\ln^2 S\right]$	$\alpha_{\mathrm{pq}}\hat{p}_{\mathrm{A}}$	$\alpha_{\mathrm{pq}}\hat{p}_{\mathrm{V}}\exp\left[-\ln^2 S\right]$
$\frac{dV}{dq}$	$\hat{q}_{\mathrm{V}}$	$\alpha_{\mathrm{pq}}\hat{p}_{\mathrm{N}}\exp\left[3\ln^2 S\right]$	$\alpha_{\mathrm{pq}}\hat{p}_{\mathrm{A}}\exp\left[\ln^2 S\right]$	$\alpha_{\mathrm{pq}}\hat{p}_{\mathrm{V}}$

The striking feature in the interconversions of PSDs is that the conversion of the median radius is similar to those for spherical cases but multiplied by coefficient α_{pq} as in Eq. (8) for a single particle case. The $y_{\mathrm{T,q}}$ conversion formulas are also similar to those for spherical cases as partly described in Eqs. (20–25) but include the coefficient $\alpha_{\mathrm{pa}}^{\pm 2}$ for conversions between the number and projected area concentrations, $\alpha_{\mathrm{pv}}^{\pm 3}$ between the number and volume concentrations, and $\alpha_{\mathrm{pe}}^{\pm 1}$ between the projected area and volume concentrations, respectively.

b. Gamma distributions

Similarly, the interconversions of GDs can be achieved by solving Eq. (40) as

$$\frac{dy(q)}{dq} = \frac{y_{\mathrm{T,q}}\Lambda_{\mathrm{q}}{}^{\mu_{\mathrm{y}}}}{\Gamma(\mu_{\mathrm{y}})}q^{\mu_{\mathrm{y}}-1}\exp\left[-\Lambda_{\mathrm{q}}q\right], \tag{42}$$

where a set of new parameters $y_{\mathrm{T,q}}$, μ_{y}, and Λ_{q} can be obtained from a set of old parameters $x_{\mathrm{T,p}}$ μ_{x}, and Λ_{p} (Table 3). Interestingly, the slope parameter is converted with $\Lambda_{\mathrm{q}} = \Lambda_{\mathrm{p}}/\alpha_{\mathrm{pq}}$ for the conversions of the size descriptor from one (p) to another (q), which is independent of the conversions of the physical variable in PSD, while the dispersion parameter is independent of the size descriptor conversion, and their conversions follow the form of those for spherical particles partly described in Eqs. (34–35). Similar to the LND cases, the physical variable conversions $y_{\mathrm{T,q}}$ include the coefficients α_{pa}, α_{pv}, or α_{pe} depending on the physical variables involved in the conversions.

Table 3. Same as Table 2, except for gamma PSDs in Eq. (42).

Parameters in the target GD		Parameters in the source GD		
		$\frac{dN}{dp}$	$\frac{dA}{dp}$	$\frac{dV}{dp}$
		$N_{\mathrm{T,p}}$	$A_{\mathrm{T,p}}$	$V_{\mathrm{T,p}}$
$\frac{dN}{dq}$	$N_{\mathrm{T,q}}$	$N_{\mathrm{T,p}}$	$\frac{1}{\pi}\alpha_{\mathrm{pa}}^{-2}A_{\mathrm{T,p}}\,\Lambda_{\mathrm{p}}^{2}\frac{1}{\prod_{i=1}^{2}(\mu_{\mathrm{A}}-i)}$	$\frac{3}{4\pi}\alpha_{\mathrm{pv}}^{-3}V_{\mathrm{T,p}}\Lambda_{\mathrm{p}}^{3}\frac{1}{\prod_{i=1}^{3}(\mu_{\mathrm{V}}-i)}$
$\frac{dA}{dq}$	$A_{\mathrm{T,q}}$	$\pi\alpha_{\mathrm{pa}}^{2}N_{\mathrm{T,p}}\Lambda_{\mathrm{p}}^{-2}\prod_{i=0}^{1}(\mu_{\mathrm{N}}+i)$	$A_{\mathrm{T,p}}$	$\frac{3}{4}\alpha_{\mathrm{pe}}^{-1}V_{\mathrm{T,p}}\Lambda_{\mathrm{p}}\frac{1}{(\mu_{\mathrm{V}}-1)}$
$\frac{dV}{dq}$	$V_{\mathrm{T,q}}$	$\frac{4}{3}\pi\alpha_{\mathrm{pv}}^{3}N_{\mathrm{T,p}}\Lambda_{\mathrm{p}}^{-3}\prod_{i=0}^{2}(\mu_{\mathrm{N}}+i)$	$\frac{4}{3}\alpha_{\mathrm{pe}}A_{\mathrm{Tp}}\Lambda_{\mathrm{p}}^{-1}\mu_{\mathrm{A}}$	$V_{\mathrm{T,p}}$
		μ_{N}	μ_{A}	μ_{V}
$\frac{dN}{dq}$	μ_{N}	μ_{N}	$\mu_{\mathrm{A}}-2$	$\mu_{\mathrm{V}}-3$
$\frac{dA}{dq}$	μ_{A}	$\mu_{\mathrm{N}}+2$	μ_{A}	$\mu_{\mathrm{V}}-1$
$\frac{dV}{dq}$	μ_{V}	$\mu_{\mathrm{N}}+3$	$\mu_{\mathrm{A}}+1$	μ_{V}

c. Radius-to-diameter conversions

Within the same type of size descriptor, a conversion of PSDs from the radius notation to the diameter notation requires (PH11)

$$\frac{dN(r)}{dr} = 2\frac{dN\left(\frac{D}{2}\right)}{dD}. \quad (43)$$

Therefore, the conversions for LND and GD in terms of the number concentrations are described by substituting Eq. (43) into Eqs. (18, 28) as

$$\frac{dN(r)}{dr} = \frac{2}{D}\frac{N_{\mathrm{T}}}{\ln S\sqrt{2\pi}}\exp\left[-\frac{1}{2}\left(\frac{\ln D - \ln 2\hat{r}_{\mathrm{N}}}{\ln S}\right)^2\right], \tag{44}$$

$$\frac{dN(r)}{dr} = \frac{2N_{\mathrm{T}}\left(\frac{\Lambda_r}{2}\right)^{\mu_{\mathrm{N}}}}{\Gamma(\mu_{\mathrm{N}})} D^{\mu_{\mathrm{N}}-1}\exp\left[-\frac{\Lambda_r}{2}D\right], \tag{45}$$

where $\widehat{D}_{\mathrm{N}} = 2\hat{r}_{\mathrm{N}}$, $S_D = S_r$, $\Lambda_D = \frac{\Lambda_r}{2}$, and $\mu_{\mathrm{N,D}} = \mu_{\mathrm{N,r}}$ through a conversion from $\frac{dN(r)}{dr}$ to $\frac{dN(D)}{dD}$. Based on the derived formulas in Sections 4a–c (Eqs. 41–45 and Tables 1–3), the ambiguity in the interconversions of PSDs for nonspherical particles can be overcome as long as the particle shape is size-invariant.

d. Effective radius of nonspherical PSD

For nonspherical particles, there were extensive discussions on the definition of the effective radius for a specified PSD (e.g., Ebert and Curry, 1992; Liou, 1992; Fu, 1996; Wyser and Yang, 1998) due to ambiguity about the particle "radius" in Eq. (16). For a PSD of nonspherical ice crystals, the following definition of the effective radius (Foot, 1988; hereinafter referred to as F88) has often been used:

$$\langle R_{\mathrm{eff}}\rangle = \frac{3\int_0^\infty v(r)\frac{dN(r)}{dr}dr}{4\int_0^\infty a(r)\frac{dN(r)}{dr}dr}, \tag{46}$$

which is mathematically equivalent to the original definition (Eq. 16) by HT74 in the case of spherical particles; in particular, substituting $v(r) = \frac{4}{3}\pi r^3$ and $a(r) = \pi r^2$ into Eq (46) gives exactly Eq. (16). In addition, Eq (46) has no ambiguous nonspherical radius r and thus is a useful definition of $\langle R_{\mathrm{eff}}\rangle$ for nonspherical particles. However, as Wyser (1998) argued, the definition of $\langle R_{\mathrm{eff}}\rangle$ must be a projected-area weighted particle radius according to the original concept of $\langle R_{\mathrm{eff}}\rangle$ introduced by HT74. From Eqs. (3, 16, 46), we find that

$$\langle R_{\mathrm{eff}}\rangle = \frac{\int_0^\infty r_{\mathrm{e}}(r)a(r)\frac{dN(r)}{dr}dr}{\int_0^\infty a(r)\frac{dN(r)}{dr}dr}, \tag{47}$$

which indicates that r_{e} should be the radius of a single nonspherical particle being weighted with the projected area for $\langle R_{\mathrm{eff}}\rangle$. Hence, Eq. (47) can be considered a generalized form of the $\langle R_{\mathrm{eff}} \rangle$ definition for arbitrary particles, as it satisfies the original concept of $\langle R_{\mathrm{eff}} \rangle$ by HT74 and is also consistent with Eq. (16) for spherical particles.

Numerous studies have applied Eq. (16) to a PSD of nonspherical particles for the $\langle R_{\mathrm{eff}} \rangle$ calculation, although the accuracy of Eq. (16) is guaranteed only for spherical particles. Therefore, we evaluate a potential systematic bias in $\langle R_{\mathrm{eff}} \rangle$ for the PSD of nonspherical particles with various size descriptors based on Eq. (16). We take the ratio of $\langle R_{\mathrm{eff}} \rangle$ defined in Eq. (16) $\langle R_{\mathrm{eff,HT74}} \rangle$ to Eq. (46) $\langle R_{\mathrm{eff,F88}} \rangle$ for a given size descriptor p, and we have

$$\frac{\langle R_{\mathrm{eff,HT74}} \rangle}{\langle R_{\mathrm{eff,F88}} \rangle} = \alpha_{\mathrm{ep}}, \tag{48}$$

where α_{ep} is a conversion coefficient from the effective radius to the given size descriptor p, as listed in Table 1. This mathematical analysis indicates that the two effective radius definitions systematically deviate from each other for nonspherical particles with $\Psi < 1$ and $\frac{V_{\mathrm{r}}}{A_{\mathrm{r}}} < 1$.

Figure 1 illustrates the systematic $\langle R_{\mathrm{eff}} \rangle$ biases of nonspherical particles defined as $\left(\langle R_{\mathrm{eff,HT74}} \rangle - \langle R_{\mathrm{eff,F88}} \rangle\right)/\langle R_{\mathrm{eff,F88}} \rangle$ with various size descriptors. Typical aerosol and ice crystal models are also shown in Fig. 1, including the droxtal (Yang et al., 2003), the hexagonal column with an aspect ratio of unity, irregular hexahedral ensemble (Saito et al., 2021), and 8-column aggregate (Yang et al., 2013). For size descriptors r_{v} and r_{a}, the systematic biases in $\langle R_{\mathrm{eff}} \rangle$ by HT74 for nonspherical particles are proportional to $\Psi^{-\frac{3}{2}}$ and Ψ^{-1}, respectively. In addition, the bias for size descriptor r_{g} is proportional to $\left(\frac{V_{\mathrm{r}}}{A_{\mathrm{r}}}\right)^{-1} > 1$. Therefore, Eq. (16) substantially overestimates $\langle R_{\mathrm{eff}} \rangle$ for typical ice crystals and aerosol models other than a droxtal, for which Eq. (16) leads to a moderate positive $\langle R_{\mathrm{eff}} \rangle$ bias as it is a quasi-spherical shape. On the other hand, using Eq. (16) for nonspherical particles with size descriptor r_{e} does not induce a systematic bias in $\langle R_{\mathrm{eff}} \rangle$, which corroborates the validity of Eq. (47). Thus, $\langle R_{\mathrm{eff}} \rangle$ must be derived from either the F88 definition (Eq. 46) or the HT74 definition with a size descriptor of r_{e} for a PSD of arbitrary nonspherical particles (Eq. 47).

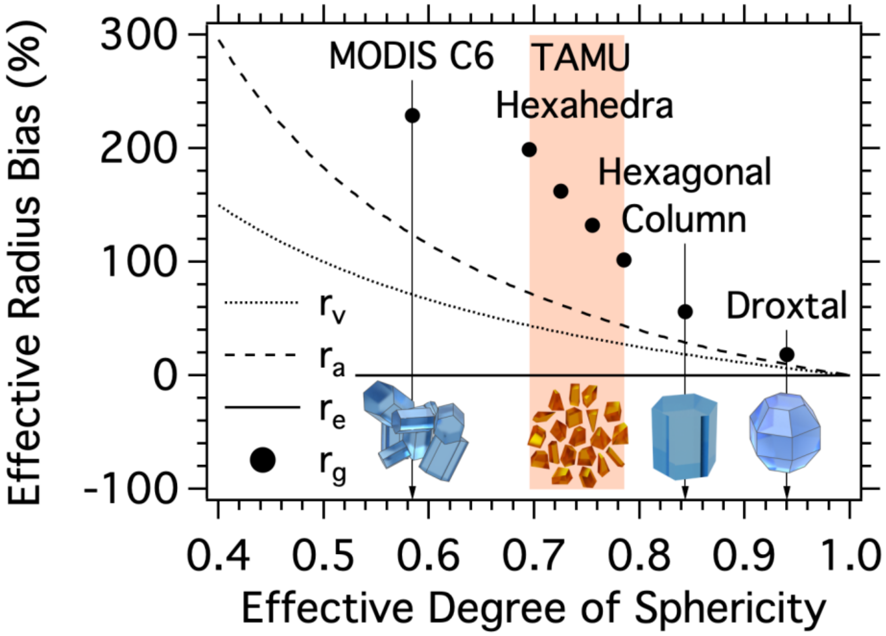

Fig. 1. Effective radius biases among size descriptors due to applying Eq. (16) for nonspherical particles. Example particle shape models include droxtal, compact hexagonal column, hexahedral ensemble, and 8-column aggregate used as a particle shape model for MODIS Collection 6 (C6).

According to Eq. (46), we can obtain PSD parameters as a function of $\langle R_{\text{eff}} \rangle$. For LND, the median radius $\hat{p}_{\text{x}}$ is described as

$$\hat{p}_{\text{N}} = \alpha_{\text{pe}} \langle R_{\text{eff}} \rangle \exp\left[-\frac{5}{2}\ln^2 S\right], \tag{49}$$

and $\hat{p}_{\text{A}}$ and $\hat{p}_{\text{V}}$ are easily obtained from Table 2. For GD, the slope parameter Λ_{p} is obtained from Eq. (42, 46) and Table 3 as

$$\Lambda_{\text{p}} = \frac{\alpha_{\text{pe}}}{\langle R_{\text{eff}} \rangle \langle V_{\text{eff}} \rangle}. \tag{50}$$

e. Example interconversions of nonspherical PSDs

Example conversions of nonspherical mineral dust PSDs are performed using LNDs with a geometric standard deviation of $S = 2.0$ (Reid et al., 2003b). Two different particle shapes obtained from irregular hexahedral ensemble models with $\Psi = 0.695$ (irregular model) and $\Psi = 0.785$ (compact model) are used for the PSD conversions (Saito et al., 2021). We consider two original PSDs with $\langle R_{\text{eff}} \rangle = 1.0$ μm and $V_{\text{T}} = 800$ μm^3 cm^{-3} for Case A, and $\hat{r}_{\text{g,N}} = 0.8$ μm and $N_{\text{T}} = 300$ cm^{-3} for Case B.

Figure 2 shows the interconversions of PSDs for two nonspherical models. Case A corresponds to numerical simulations of atmospheric cloud-aerosol fields, as a typical predicted quantity of atmospheric particles is the particle mass mixing ratio proportional to V_{T}. Depending on the size descriptor, the peaks of PSDs (i.e., $\hat{p}_{\mathrm{x}}$) deviate from each other model by a factor of the ratio of α_{pe} between two nonspherical models according to Eq. (49). The two nonspherical models have identical PSDs for $dA/d\ln r_{\mathrm{e}}$ and $dV/d\ln r_{\mathrm{e}}$ (Fig. 2h), as the original PSDs have the same $\langle R_{\mathrm{eff}}\rangle$ (Fig. 2g). Also, all PSDs show a consistent A_{T}, as $\langle R_{\mathrm{eff}}\rangle$ and V_{T} are consistent for Case A. N_{T} is systematically larger for the compact model ($\Psi = 0.785$) than for the irregular model ($\Psi = 0.695$) by a factor of the cube of the α_{pv} ratio, or $(0.785/0.695)^3 \approx 1.441$ according to Table 1.

Case B is typical for the *in-situ* measurements of PSDs using a Differential Mobility Particle Sizer (e.g., Schladitz et al., 2009). The PSDs converted from the original PSD $dN/d\ln r_{\mathrm{g}}$ to the other size descriptors show a systematic shift of $\hat{p}_{\mathrm{x}}$ toward smaller sizes using the irregular model than the compact model. In addition, these PSDs also show systematically larger A_{T} and V_{T} for the compact model, compared to the irregular model, by a factor of the square of the α_{pa} ratio and the cube of the α_{pv} ratio, respectively (see Table 2). This inconsistency was also suggested by PH11, which shows marked differences among PSD parameterizations of snow with the same snow water content. However, a major point relevant to this paper is that converted PSDs $dY/d\ln q$ can differ among nonspherical particle models even though the original PSDs $dX/d\ln p$ among these models are identical, as demonstrated in Fig. 2. In addition, the deviations of PSDs can be analytically derived for arbitrary nonspherical particles with coefficient α, as specified in Tables 1–3.

Accepted for publication in *Journal of the Atmospheric Sciences.* DOI 10.1175/JAS-D-22-0086.1.

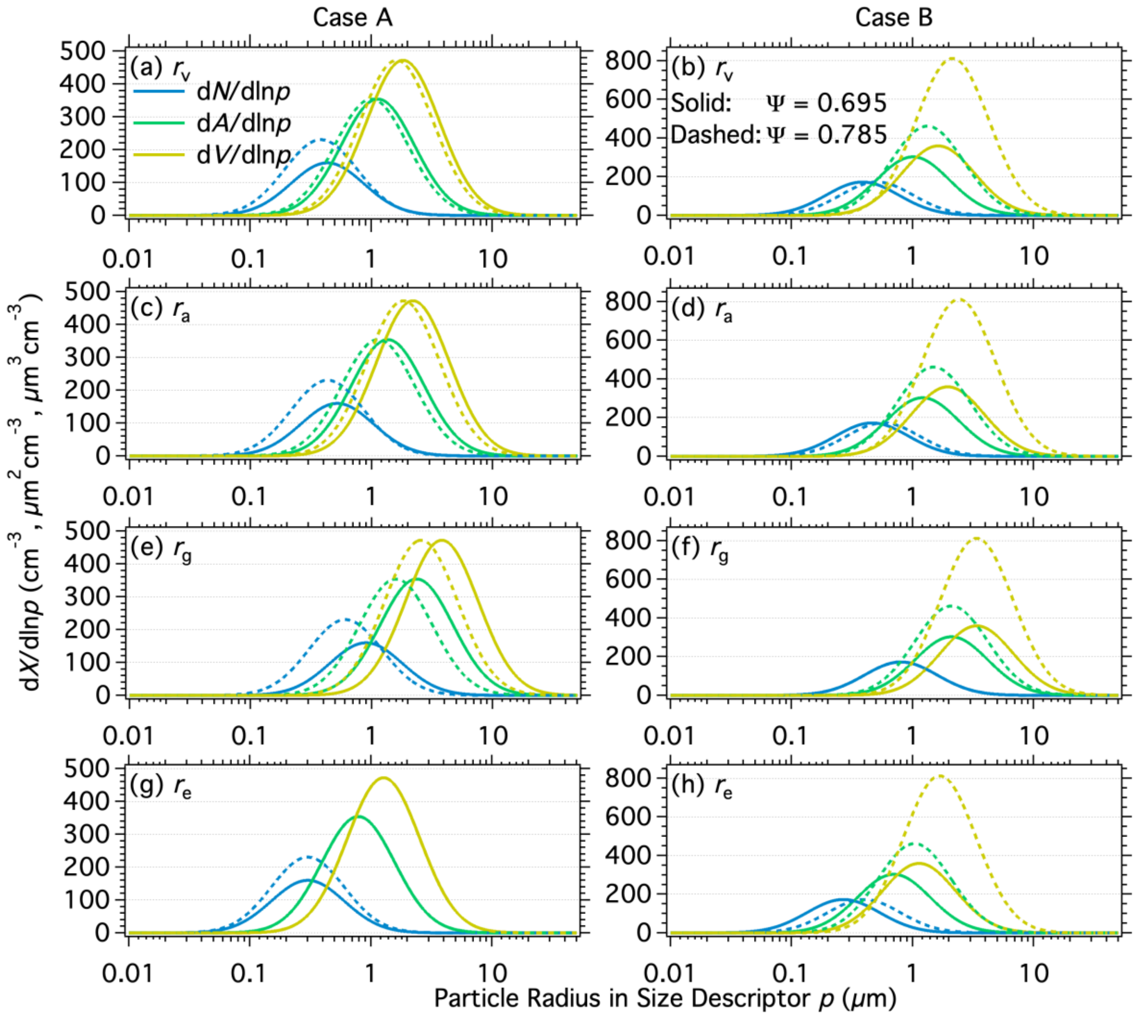

Fig. 2. Converted log-normal PSDs in terms of (blue) the number, (green) projected area, and (yellow) volume concentrations with respect to the size descriptors of (a-b) the volume-equivalent spherical radius, (c-d) projected area-equivalent spherical radius, (e-f) geometric radius, and (g-h) effective radius. Solid and dashed lines are for the irregular and compact models, respectively. The original PSDs are $dA/d\ln r_\mathrm{e}$ for Case A and $dV/d\ln r_\mathrm{e}$ for Case B.

f. Example analysis of in-situ measured nonspherical PSDs

We performed another example analysis of ice cloud PSDs using airborne *in-situ* observations compiled by Heymsfield et al. (2013), consisting of 78 flights among 10 observational campaigns targeting ice clouds. In each airborne observation, an ice cloud PSD is fitted with a gamma PSD using the maximum diameter as the size descriptor. The dataset contains the slope parameter, dispersion parameter, and intercept in addition to meteorological variables such as temperature. We exclude the measured PSDs with temperatures warmer than -40°C from the analysis to avoid potential biases by inclusion of liquid droplets. In total, we analyze 14,405 PSDs to estimate $\langle R_{\mathrm{eff}} \rangle$ and $\langle V_{\mathrm{eff}} \rangle$ of ice clouds from *in-situ* measured PSDs.

Figure 3 shows the occurrence density of $\langle R_{\mathrm{eff}} \rangle$ and $\langle V_{\mathrm{eff}} \rangle$ of ice clouds. For gamma PSDs, $\langle V_{\mathrm{eff}} \rangle$ can be estimated from the dispersion parameters through Eq. (37), showing a median value of ~0.26 that is larger than that for liquid clouds (~0.1; Miles et al., 2000). The effective radius is obtained from Eq. (36) for a gamma PSD (Eq. 38) originally derived from HT74, as shown in Fig. 3b. Significantly larger $\langle R_{\mathrm{eff}} \rangle$ values, ranging mostly from 80–200 µm, are obtained due to an assumption of spherical particles in Eq. (38). We estimate $\langle R_{\mathrm{eff}} \rangle$ from the same dataset using Eq. (50) under the assumption of the MODIS C6 ice model as a nonspherical ice crystal shape, showing a reasonable range of $\langle R_{\mathrm{eff}} \rangle$ 30–70 µm, which is fairly consistent with climatology inferred from spaceborne observations (Platnick et al., 2016). Therefore, an incorporation of the particle nonsphericity into *in-situ* measured PSD analysis is essential.

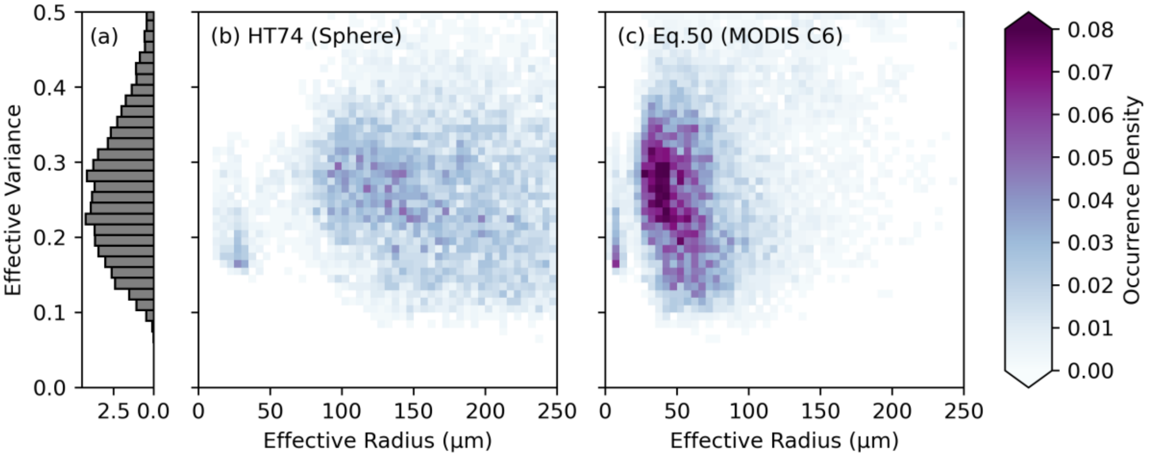

Fig. 3. (a) A histogram of the effective variance, (b-c) two-dimensional histograms of the effective radius and variance of ice clouds derived from *in-situ* measured particle size distributions based on Eq. (36) originally derived by HT74 and Eq. (50) that incorporates the nonspherical shape effects, respectively.

g. A practical form for an arbitrary PSD with size-dependent nonspherical particles

Analytical interconversions of two PSDs derived in the previous sections rely on the assumption of size-invariant particle shapes. In reality, the size distributions of atmospheric particles may not always be fitted well with these analytical PSD formulas.

The *in-situ* measurements of PSDs are depicted using a limited number of discretized size bins (e.g., Reid et al., 2003a). In addition, atmospheric particles show size-dependent particle shapes, as confirmed by *in-situ* observations of ice crystals (e.g., Ono, 1970; Lawson et al., 2019) and mineral dust particles (e.g., Reid et al., 2003b). To incorporate these observational PSDs of size-dependent nonspherical atmospheric particles, more practical formulation of the interconversions of arbitrary PSDs is desirable.

Let an arbitrarily discretized PSD be $\frac{\Delta x_i}{\Delta p_i}$, where Δx_i is the total amount of a physical variable (i.e., N, A, or V) of nonspherical particles whose size p falls within particle size bin *i* (indicated as subscript *i*), $\left[p_{\mathrm{min},i}, p_{\mathrm{max},i}\right]$ with a finite bin width of $\Delta p_i = p_{\mathrm{max},i} - p_{\mathrm{min},i}$. We consider a conversion of PSD from $\frac{\Delta x_i}{\Delta p_i}$ into $\frac{\Delta y_i}{\Delta q_i}$. The particle shape (i.e., Ψ, V_r, and A_r) varies across size bins but is assumed to be homogeneous within a size bin. Also, the number concentration within a size bin is assumed to be homogeneous. The conversions of an arbitrary PSD in size bin *i* can be given as

$$\frac{\Delta y_i}{\Delta q_i} = f_{\mathrm{xy},i}\alpha_{\mathrm{pq},i}^{-1}\frac{\Delta x_i}{\Delta p_i}, \tag{51}$$

where a coefficient for the interconversions of a physical variable from x to y for a PSD $f_{\mathrm{xy},i}$ obeys

$$f_{\mathrm{yx},i} = f_{\mathrm{xy},i}^{-1}, \tag{52}$$

$$f_{\mathrm{NA},i} = \int_{p_{\mathrm{min},i}}^{p_{\mathrm{max},i}} \pi\tilde{p}^2\alpha_{\mathrm{pa},i}^2 d\tilde{p} = \frac{\pi\alpha_{\mathrm{pa},i}^2}{3}\left(p_{\mathrm{max},i}^2 + p_{\mathrm{max},i}p_{\mathrm{min},i} + p_{\mathrm{min},i}^2\right), \tag{53}$$

$$f_{\mathrm{NV},i} = \int_{p_{\mathrm{min},i}}^{p_{\mathrm{max},i}} \frac{4}{3}\pi\tilde{p}^3\alpha_{\mathrm{pv},i}^3 d\tilde{p} = \frac{\pi\alpha_{\mathrm{pv},i}^3}{3}\left(p_{\mathrm{max},i}^2 + p_{\mathrm{min},i}^2\right)\left(p_{\mathrm{max},i} + p_{\mathrm{min},i}\right), \tag{54}$$

$$f_{\mathrm{AV},i} = f_{\mathrm{NV},i}f_{\mathrm{NA},i}^{-1} = \alpha_{\mathrm{pe}}\frac{\left(p_{\mathrm{max},i}^2+p_{\mathrm{min},i}^2\right)\left(p_{\mathrm{max},i}+p_{\mathrm{min},i}\right)}{p_{\mathrm{max},i}^2+p_{\mathrm{max},i}p_{\mathrm{min},i}+p_{\mathrm{min},i}^2}. \tag{55}$$

The above formulas would be useful particularly for converting *in-situ* measured PSDs from one to another form when collocated size-resolved particle shape measurements are available.

5. The Impacts on the Optical Properties

Understanding the impact of a choice of the size descriptor on the simulations of the single-scattering properties of nonspherical particles is critical to radiative transfer applications. The definition of size parameter kr is extended to a nonspherical particle by replacing a radius of a sphere with a size descriptor of a nonspherical particle, where various size descriptors are arbitrarily selected in the literature. A different size descriptor could affect the comparisons of the single-scattering properties among various nonspherical particles with the same size parameter value for investigating the impacts of particle shapes on the scattering properties. This is because the volume, projected area, and these relations can be different among the nonspherical particle size descriptors.

Hence, it is important to choose the best size descriptor for the size parameter that achieves the same optical size (hereinafter referred to as optically quasi-equivalent size) among various nonspherical particles. An earlier study by GW99 suggests kr_{e} as the best size descriptor through a comparison of the scattering properties between spherical and nonspherical particles. Here, we revisit the predefined four size descriptors for the size parameter definitions (kr_{v}, kr_{a}, kr_{g}, and kr_{e}) and discuss a possible mechanism behind the optically quasi-equivalent size among nonspherical particles.

a. Single-scattering properties

To determine the best size descriptor for the size parameter of a nonspherical particle, we compute the single-scattering properties of three nonspherical mineral dust particles, including compact, moderately, and severely irregular hexahedral particle models obtained from the TAMUdust2020 database (Saito et al., 2021; particle IDs 20, 11, and 01, respectively). The single-scattering property simulations of these nonspherical particles are performed with the Invariant-Imbedding T-matrix Method (IITM; Johnson, 1988; Bi et al., 2013) for geometric size parameter $kr_{\mathrm{g}} \leq 75$ and the Improved Geometric Optics Method (IGOM; Yang and Liou, 1996) for larger kr_{g}. The complex refractive index of dust with the real part $m_{\mathrm{r}} = 1.5$ and the imaginary part $m_{\mathrm{i}} = 0.001$, typical in the shortwave, is selected for the evaluation of the optically quasi-equivalent size.

Figure 4 shows the single-scattering properties of these three nonspherical dust particles with size parameters ranging from 1–70 for these four size descriptors. The extinction efficiency Q_{ext} of nonspherical particles has two striking features. First, peaks of Q_{ext} due to optical interference between diffracted and refracted waves of light by a particle appear at different size parameters among the size descriptors (Figs. 4a-d).

Accepted for publication in *Journal of the Atmospheric Sciences.* DOI 10.1175/JAS-D-22-0086.1.

Second, the optical interference patterns tend to be coherent among the three nonspherical models with the kr_e size descriptor (Fig. 4d). The single-scattering albedo (SSA; ω) is also consistent among the three nonspherical particle models using kr_e (Fig. 4h) compared to other size descriptors (Figs. 4e-g). This implies that an optically quasi-equivalent size for the three nonspherical particles is achieved using kr_e due to the consistent phase shift and light absorption by refracted waves in those nonspherical particles. The rest of this section is a detailed exploration of this implication, including tests involving other particle shapes and ice particles in addition to aerosols.

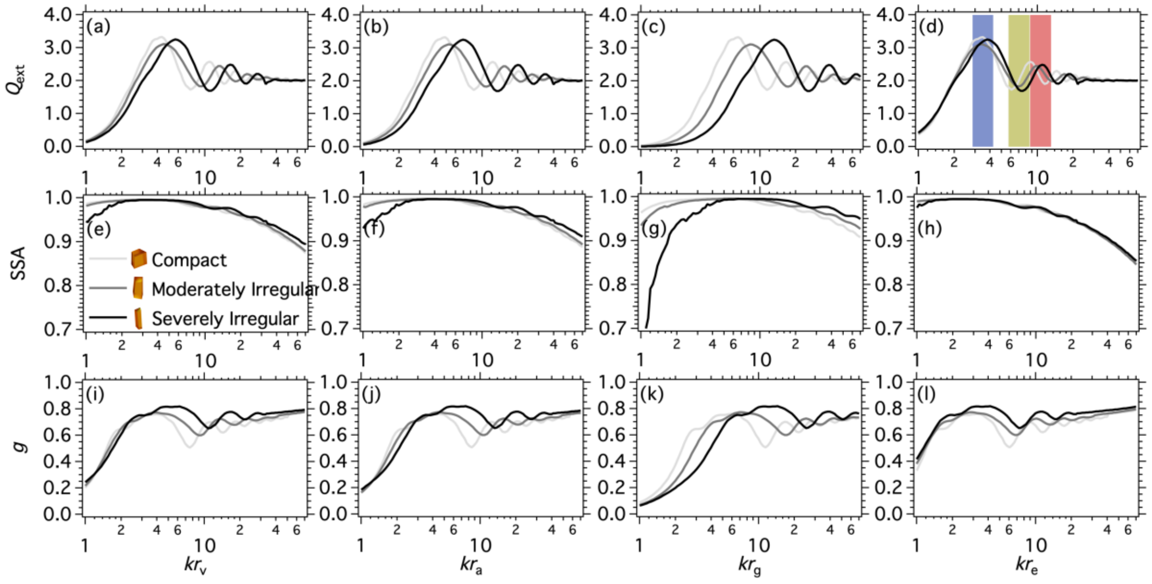

Fig. 4. (a-d) The extinction efficiency, (e-h) single-scattering albedo, and (i-l) asymmetry factor of nonspherical particles for size parameters 1-70 defined with (first column) the volume-equivalent spherical radius, (second column) projected-area-equivalent spherical radius, (third column) geometric radius, and (fourth column) effective radius. Lines indicate three nonspherical dust particle models. Blue, yellow, and red color shades in (d) correspond to the range of the first, second, and third peaks of the extinction efficiency predicted with a modified anomalous diffraction theory.

Therefore, a kr_e size parameter is the best choice for comparing the single-scattering properties of different nonspherical particles with the same size parameter, which is consistent with GW99. In other words, comparisons of the single-scattering property simulations among nonspherical particles based on other size descriptors could complicate the interpretation of the results, as the single-scattering property differences are associated with both size and shape differences. The asymmetry factor g exhibits systematic differences for all size descriptor cases, including the kr_e cases that purely show the sensitivity of g to the particle shape.

b. Possible physical rationale

We explore a possible theoretical rationale of the optically quasi-equivalent size achieved with kr_e for nonspherical particles. To explain the coherent oscillation of Q_ext and consistent SSA for these nonspherical particles in a physics-based manner, we shall recall the anomalous diffraction theory (ADT) originally developed by Van de Hulst (1957) for optically soft particles (i.e., $|m_r - 1| \ll 1$). In principle, ADT is not applicable to typical atmospheric nonspherical particles when m_r is not close to 1 because of the assumption of the rectilinear propagation of the incident wave though the scattering particle. However, the essential mechanism of the coherent oscillation of Q_ext in such particles as seen in Fig. 4 is quite similar to ADT (Bi and Gouesbet, 2022), except the optical interference between diffraction and transmitted waves propagating in the forward direction.

Reformulating ADT in terms of the probability density of the geometric-path length (l) of a randomly oriented particle (Xu et al., 2003; Yang et al., 2004), the extinction and absorption cross-sections are written as

$$C_\mathrm{ext} = 2a\int_0^\infty \{1 - \exp(-kl^* m_\mathrm{i})\cos[kl^*(m_\mathrm{r} - 1)]\} h(l^*)\,dl^*, \tag{56}$$

$$C_\mathrm{abs} = a\int_0^\infty [1 - \exp(-2kl^* m_\mathrm{i})] h(l^*)\,dl^*, \tag{57}$$

where $h(l^*)$ is the geometric-path length distribution of a randomly oriented particle. Xu et al. (2003) assume that the geometric-path length distribution obeys the Gaussian distribution, $N(\mu, \sigma)$, and solve Eqs. (56–57) by replacing the lower boundary of l^* with $-\infty$ [see Eq. 10 in Xu et al. (2003)] as follows:

$$C_\mathrm{ext} = 2a - 2a\cos[k(m_\mathrm{r} - 1)(\mu - k\sigma^2 m_\mathrm{i})]\exp\left\{-k\mu m_\mathrm{i} - \frac{k^2\sigma^2[(m_\mathrm{r}-1)^2 - m_\mathrm{i}^2]}{2}\right\}, \tag{58}$$

$$C_\mathrm{abs} = a\{1 - \exp[-2km_\mathrm{i}(\mu - k\sigma^2 m_\mathrm{i})]\}. \tag{59}$$

For a convex particle, the mean geometric-path length ($\bar{l}$) is proportional to the ratio of the volume to the projected area of a particle ($\bar{l} = v/a$), which is theoretically derived for diffusive media (Blanco and Foumier, 2003) and experimentally indicated for non-diffusive media (Davy et al., 2021). From Eq. (3), we have

$$\bar{l} = \frac{4}{3} r_\mathrm{e}. \tag{60}$$

Based on the optical theorem, C_ext is determined at the exact forward direction, where the diffracted and the second-order forward-transmitted rays (refracted twice at the entering and exit points on the surface of a particle) are dominant according to analysis with the Debye series expansion of the phase function of a nonspherical particle (Xu et al., 2010; Bi et al., 2018). The mean geometric-path lengths of second-order transmitted rays ($\bar{l}_2$) can be larger than $\bar{l}$ because $\bar{l}$ includes short geometric-ray paths originating from incident rays at large incident angles on the particle surface, which could be reflected or transmitted toward off-forward directions for particles with a sufficiently large m_r. The longest possible geometric-ray path length is obviously $2r_\mathrm{g} = 2\left(\frac{V_\mathrm{r}}{A_\mathrm{r}}\right)^{-1} r_\mathrm{e} \geq 2r_\mathrm{e}$, where the equivalence is satisfied for the spherical case. For simplicity, we assume a possible range of $\frac{4}{3} r_\mathrm{e} \leq \bar{l}_2 \leq 2r_\mathrm{e}$. The standard deviation of the second-order transmitted rays may depend on the particle geometry but is approximated as $\frac{1}{3}\bar{l}_2$ in this study. Thus, based on Eqs. (58–59), $\frac{4}{3} \leq c_2 \leq 2$, and $h(l^*) = N\left(\bar{l}_2, \frac{1}{3}\bar{l}_2\right)$, the extinction and absorption efficiencies are obtained as

$$Q_\mathrm{ext} = 2 - 2\cos\left[(m_\mathrm{r} - 1)\left(c_2 k r_\mathrm{e} - \frac{c_2^2 k^2 r_\mathrm{e}^2 m_\mathrm{i}}{9}\right)\right] \exp\left\{-c_2 k r_\mathrm{e} m_\mathrm{i} - \frac{c_2^2 k^2 r_\mathrm{e}^2\left[(m_\mathrm{r}-1)^2 - m_\mathrm{i}^2\right]}{18}\right\}, \tag{61}$$

$$Q_\mathrm{abs} = 1 - \exp\left[-2c_2 k r_\mathrm{e} m_\mathrm{i}\left(1 - \frac{c_2 k r_\mathrm{e} m_\mathrm{i}}{9}\right)\right], \tag{62}$$

which indicates that both Q_ext and SSA $[\omega = (Q_\mathrm{ext} - Q_\mathrm{abs})/Q_\mathrm{ext}]$ are a function of kr_e. Note that the amplitude of the Q_ext oscillation in Eq. (61) may be uncertain as the exact l_2 distribution is not considered. However, the optical interference pattern should be roughly consistent as it is primarily determined by the mean optical path of rays that cause interference.

The peaks of the optical interference appear at size parameters where the derivative of Eq. (61) with respect to kr_e satisfies $\frac{dQ_\mathrm{ext}}{d(kr_\mathrm{e})} = 0$. With the uncertainty range of $\bar{l}_2$, the predicted kr_e corresponding to the first three peaks based on Eq. (61) for the present dust models are 2.84–4.25, 5.72–8.58, and 8.67–13.01 as specified in Fig. 4d, which are reasonably consistent with rigorously computed Q_{ext} for the three nonspherical particles.

c. The bulk optical properties

An arbitrary choice of the size descriptor should not numerically affect any quantities that are weighted with a PSD such as the bulk optical properties of nonspherical particles for the same PSD. Let $\frac{dN(p)}{dp}$ be an original log-normal PSD and be convertible to $\frac{dA(q)}{dq}$. The bulk extinction efficiency at a single wavelength is derived from a PSD with any size descriptor q as

$$\langle Q_{\mathrm{ext}} \rangle = \frac{\int_0^\infty Q_{\mathrm{ext}}(q) \frac{dA(q)}{dq} dq}{\int_0^\infty \frac{dA(q)}{dq} dq}. \tag{63}$$

As an original PSD of $\frac{dA(q)}{dq}$ among size descriptors q is the same PSD, the total projected area concentration and median radius of $\frac{dA(q)}{dq}$ are expressed with size descriptor p as $A_{\mathrm{T,q}} = \pi \hat{p}_{\mathrm{N}}^2 \alpha_{\mathrm{pq}}^2 N_{\mathrm{T}} \exp[2 \ln^2 S]$ and $\hat{q}_{\mathrm{A}} = \alpha_{\mathrm{pq}} \hat{p}_{\mathrm{N}} \exp[2 \ln^2 S]$.

If $q(p) = \alpha_{\mathrm{pq}} p$, then Eq. (63) can be reformulated as

$$\langle Q_{\mathrm{ext}} \rangle = \frac{\int_0^\infty Q_{\mathrm{ext}}[q(p)] \frac{dA[q(p)]}{dq} \frac{dN_q}{dA_q} \frac{dq}{dp} dp}{\int_0^\infty \frac{dA[q(p)]}{dq} \frac{dN_q}{dA_q} \frac{dq}{dp} dp} = \int_0^\infty Q_{\mathrm{ext}}(p) \frac{dn(p)}{dp} dp, \tag{64}$$

where $\frac{dn(p)}{dp}$ is a normalized log-normal PSD with a median radius of $\hat{p}_{\mathrm{N}} \exp[2 \ln^2 S]$. This mathematically proves that $\langle Q_{\mathrm{ext}} \rangle$ is identical for the same PSD with different size descriptors. This is valid not only for $\langle Q_{\mathrm{ext}} \rangle$ but also other bulk optical properties including $\langle \omega \rangle$, $\langle g \rangle$, and $\langle P \rangle$. Thus, a choice of the size descriptor for the size parameter does not cause an error in the bulk optical property calculations, as long as the size descriptors of nonspherical particles are consistent between the size parameter for the single-scattering property simulation and a PSD.

d. Optical quasi-equivalence

As discussed in Sections 5a–b, different nonspherical particles with an optically quasi-equivalent size show fairly consistent Q_{ext} and SSA. It would be of interest to explore another group of different nonspherical particles that have quasi-equivalent single-scattering properties among them, including g and P (hereinafter referred to as optical quasi-equivalence). As it is practically difficult to simulate the scattering properties of a complex geometric particle using some light-scattering computational techniques, optical quasi-equivalence could be useful by modeling these scattering properties with a simpler geometric particle model. This study examines the optical quasi-equivalence by comparing the single-scattering properties among three roughened ice crystal models.

1) SURFACE ROUGHNESS MODELS

The degree of surface roughness is defined in terms of the variance (σ^2) of the two-dimensional (2D) Gaussian distribution of particle surface tilt angles (Cox and Munk, 1954; Yang and Liou, 1998), which describes the statistical distribution of the slope of a local planar face of a particle:

$$P(Z_x, Z_y) = \frac{1}{\pi\sigma^2} e^{-[(Z_x^2+Z_y^2)/\sigma^2]}, \tag{65}$$

where $Z_x = \partial Z/\partial x$ and $Z_y = \partial Z/\partial y$ are the slopes of a local particle surface along two axes orthogonal to the normal direction Z relative to the local planar particle surface.

The surrogate surface roughness model is often used for light-scattering computations based on the geometric optics principle (Yang and Liou, 1998), which incorporates a random tilt of the particle surface in each surface interaction with a ray of light through the ray-tracing process in the light scattering computations (Fig. 5a). A local particle surface is tilted based on the following two angles:

$$\varphi_{\mathrm{local}} = 2\pi\xi_1, \tag{66}$$

$$\theta_{\mathrm{local}} = \cos^{-1}[1/(1-\sigma^2 \ln \xi_2)], \tag{67}$$

which obey the degree of surface roughness defined in Eq. (65) and two random numbers $(\xi_1, \xi_2) \in [0,1]$ that have uniform distributions. Hence, the slopes of a local particle surface are described as $Z_x = \partial Z/\partial x$ and $Z_y = \partial Z/\partial y$ in Eq. (65).

The geometric surface roughness model (Liu et al., 2013) is applicable to both semi-analytical and geometric optics light-scattering solvers, which explicitly consider the 3D geometry of a roughened particle surface as illustrated in Fig. 5b. A regular ice crystal particle face is split into many microscale facets (N_{facet}), and each facet is randomly tilted based on the two angles equivalent to Eqs. (66–67), as described in Liu et

Accepted for publication in *Journal of the Atmospheric Sciences.* DOI 10.1175/JAS-D-22-0086.1.

al. (2013). Therefore, a random tilt of a microscopic facet of the particle surface obeys the degree of surface roughness through Eq. (65). This study uses $N_{\mathrm{facet}} = 40$.

Liu et al. (2014) developed an irregularly distorted hexagonal ensemble model to mimic a surface roughness effect on the single-scattering property computations (Fig. 5c). Each facet of a regular ice crystal is tilted based on the two angles (φ_{macro} , θ_{macro}) equivalent to Eqs. (66–67), which alters a macroscopic shape of an ice crystal (referred to as an irregularly distorted ice crystal). The single-scattering properties of a roughened ice crystal are computed with the ensemble of those irregularly distorted ice crystals as

$$Q_{\mathrm{ext,ens}} = \frac{\sum_i^{N_{\mathrm{ens}}} Q_{\mathrm{ext,i}} a_i}{\sum_i^{N_{\mathrm{ens}}} a_i}, \tag{68}$$

$$\omega_{\mathrm{ens}} = \frac{\sum_i^{N_{\mathrm{ens}}} \omega_{\mathrm{i}} Q_{\mathrm{ext,i}} a_i}{\sum_i^{N_{\mathrm{ens}}} Q_{\mathrm{ext,i}} a_i}, \tag{69}$$

$$g_{\mathrm{ens}} = \frac{\sum_i^{N_{\mathrm{ens}}} g_{\mathrm{i}} \omega_{\mathrm{i}} Q_{\mathrm{ext,i}} a_i}{\sum_i^{N_{\mathrm{ens}}} \omega_{\mathrm{i}} Q_{\mathrm{ext,i}} a_i}, \tag{70}$$

$$P_{\mathrm{ens}} = \frac{\sum_i^{N_{\mathrm{ens}}} P_{\mathrm{i}} \omega_{\mathrm{i}} Q_{\mathrm{ext,i}} a_i}{\sum_i^{N_{\mathrm{ens}}} \omega_{\mathrm{i}} Q_{\mathrm{ext,i}} a_i}, \tag{71}$$

where the number of ensemble members $N_{\mathrm{ens}} = 50$ is used in this study. The irregularly distorted ice crystals have the same r_{e} to achieve the optically quasi-equivalent size.

As the random tilt process in these three roughness models obeys the same equation that is a function of the degree of surface roughness, these three roughness models can overall be mathematically comparable. The difference among the three roughness models is the geometric scale of the surface roughness, where the surrogate roughness, geometric roughness, and irregularly distorted ensemble models account for infinitesimally small scale, $2r_{\mathrm{g}}/N_{\mathrm{facet}}$-scale, and $2r_{\mathrm{g}}$-scale of roughness, respectively.

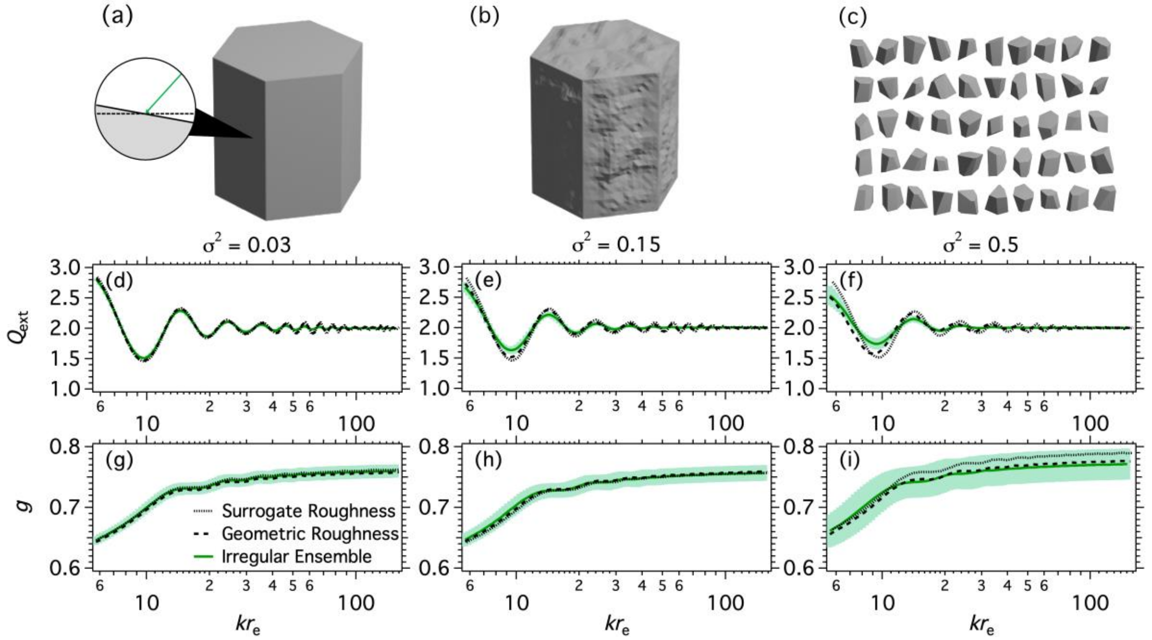

Fig. 5. An illustration of three ice crystal roughness models, including (a) surrogate roughness model, (b) geometric roughness model, and (c) irregularly distorted ensemble models for the case with $\sigma^2 = 0.15$. (d-f) The extinction efficiencies and (g-i) the asymmetry factors of the three ice crystal roughness models for degrees of surface roughness of (left column) 0.03, (center column) 0.15, and (right column) 0.5. The light green shaded area shows the weighted standard deviation of 50 irregularly distorted ensemble members.

2) SINGLE-SCATTERING PROPERTY COMPARISONS

To examine consistency among the three ice crystal roughness models based on the geometric optics principles, we compute the single-scattering properties of these models with IGOM (Yang and Liou, 1996) at a wavelength of 0.65 μm and an ice refractive index of ($m_r = 1.308$, $m_i = 1.43e^{-9}$). Figures 5d-i compare the single-scattering properties among the roughness models for degrees of surface roughness 0.03, 0.15, and 0.5. The Q_{ext} of these three models are generally consistent for all surface roughness cases, which corroborates the optically quasi-equivalent size. The amplitude of the Q_{ext} oscillation pattern is slightly smaller for the irregularly distorted ensemble model than for the other two roughness models.

The asymmetry factor is almost identical among the three roughness models for the three roughness cases, except for the surrogate roughness model with $\sigma^2 = 0.5$ (Fig. 5i), where the asymmetry factor is systematically higher than the other two roughness models. This is because the random surface tilt procedure occasionally provides unphysical geometric relations between the incident ray and particle surface, which leads to a skewed 2D slope distribution of the particle surface (Hioki, 2018). Noteworthily, the weighted standard deviation σ_w of the asymmetry factor increases with increasing degree of surface roughness for the irregularly distorted ensemble model, implying the significant sensitivity of the asymmetry factor to the macroscopic shape of a particle. Note that the uncertainty of the estimated ensemble-weighted optical properties is about $\sigma_w/\sqrt{N_{\mathrm{ens}}}$ according to the central limit theorem.

Figure 6 compares the full phase matrix elements of the three ice crystal roughness models for three surface roughness cases with a size parameter of $kr_{\mathrm{e}} = 150$. The full phase matrix elements are almost identical for the $\sigma^2 = 0.03$ cases and fairly consistent for the $\sigma^2 = 0.15$ cases among the three roughnesses, which demonstrate the optical quasi-equivalence. With $\sigma^2 = 0.5$, the three roughness models exhibit similar angular distributions of the phase matrix elements but systematic deviations appear in a few scattering angle ranges, such as a systematically higher P_{11} at scattering angles 40–60° with the ensemble model than the other models. Interestingly, the weighted standard deviation of the phase matrix elements of the ensemble model is inhomogeneous along the scattering angle. This indicates that the phase matrix elements at the scattering angles where σ_w is relatively larger are sensitive to the macroscopic particle shape, including, for instance, 10–30° and >120° for P_{11} and 40–160° for $-P_{12}/P_{11}$ (van Diedenhoven et al., 2012; Hioki et al., 2016). Note that the large uncertainty of the quasi-backscattering properties is not discussed here as IGOM simulations at such backscattering angles (i.e., 178°–180°) are inaccurate due to an inherent limitation.

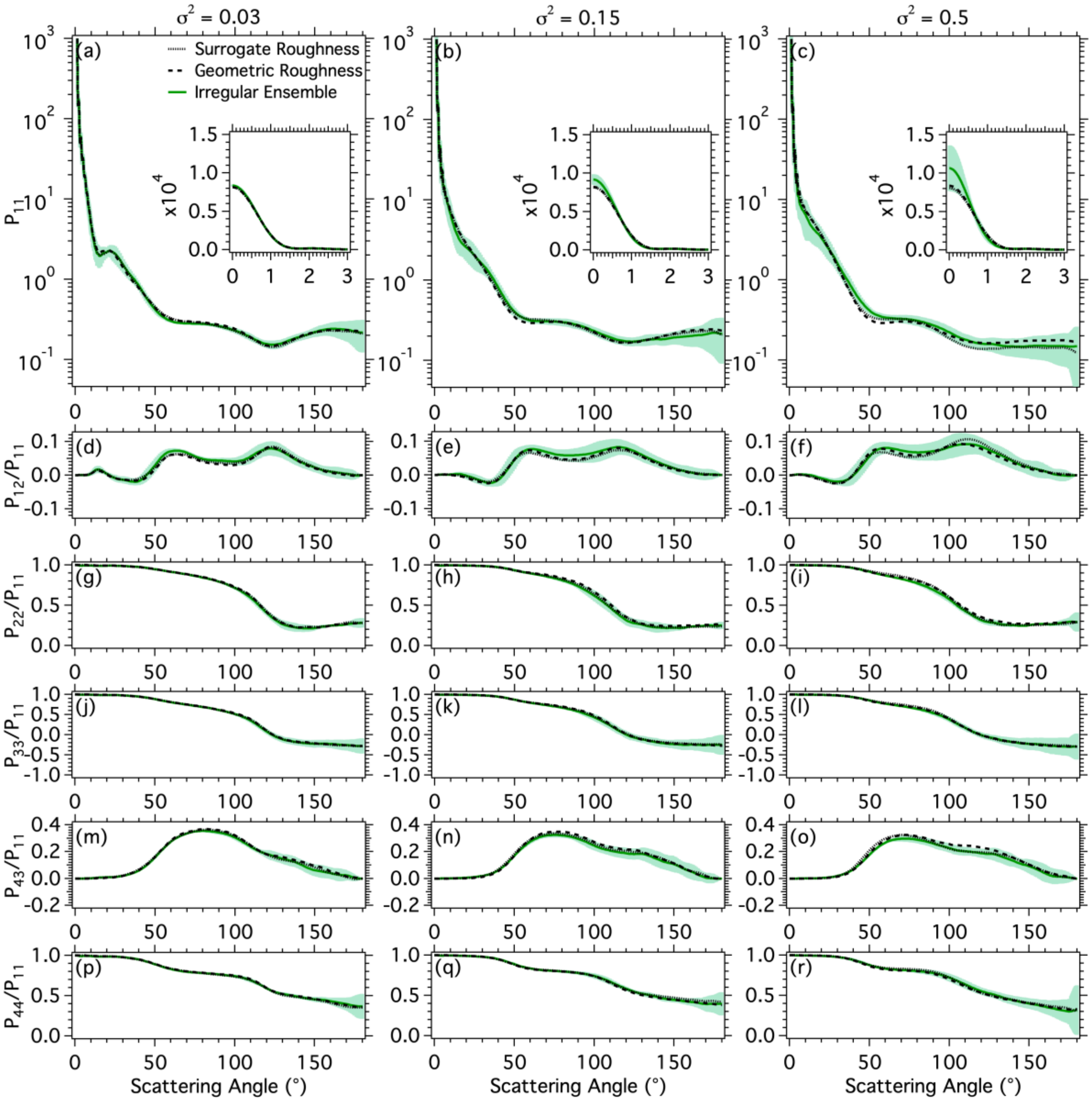

Fig. 6. Phase matrix elements of roughened ice crystal models with degree of surface roughness of (left column) 0.03, (center column) 0.15, and (right column) 0.5. Each row corresponds to (a–c) P_{11}, (d-f) -P_{12}/P_{11}, (g-i) P_{22}/P_{11}, (j-l) P_{33}/P_{11}, (m-o) P_{43}/P_{11}, and (p-r) P_{44}/P_{11}. The size parameter kr_e is 150. The light green shaded area shows the weighted standard deviation of 50 irregularly distorted ensemble members.

Importantly, the consistency of P_{11} at quasi-forward scattering angles (i.e., 0°–1°) between the ensemble and other roughness models is not achieved, as clearly seen in Figs. 6a–c. This is because P_{11} at the quasi-forward direction is mainly determined by diffraction where the scattering intensity is roughly a function of a particle projected area.

Accepted for publication in *Journal of the Atmospheric Sciences.* DOI 10.1175/JAS-D-22-0086.1.

The projected area a_{ens} and volume v_{ens} of the ensemble model with particle size r_{e} are described, based on Table 1, as

$$a_{\mathrm{ens}} = \frac{1}{N_{\mathrm{ens}}} \sum_i^{N_{\mathrm{ens}}} a_i = \pi \widetilde{\Psi}^{-3} r_{\mathrm{e}}^2, \tag{72}$$

$$v_{\mathrm{ens}} = \frac{1}{N_{\mathrm{ens}}} \sum_i^{N_{\mathrm{ens}}} v_i = \frac{4}{3} \pi \widetilde{\Psi}^{-3} r_{\mathrm{e}}^3, \tag{73}$$

where the representative degree of sphericity of the ensemble model ($\widetilde{\Psi}$) is

$$\widetilde{\Psi}^{-3} = \frac{1}{N_{\mathrm{ens}}} \sum_i^{N_{\mathrm{ens}}} \Psi_i^{-3}. \tag{74}$$

As the random surface tilt process always gives lower Ψ_i than Ψ of a regular hexagonal column, $\widetilde{\Psi} < \Psi$. This implies that a_{ens} and v_{ens} are larger than a and v of other models by a factor of $\left(\Psi/\widetilde{\Psi}\right)^3$, which becomes larger for larger σ^2. In consequence, the forward intensity is larger for a larger σ^2 for the ensemble model, as seen in Figs. 6a–c. The inconsistent geometric properties from the ensemble model indicated in Eqs. (72–74) need to be corrected for radiative transfer simulations, which is also suggested for spherical particles used as surrogates of nonspherical particles (GW99).

6. Summary and Implications

This study investigated the impacts of different size descriptors on quantifying the physical and optical properties of atmospheric nonspherical particles. Analytical expressions of the interconversions of PSD of nonspherical particles with various physical variables and size descriptors are derived for LND and GD (Eqs. 41–42, Tables 2–3, and Fig. 2), which eliminate the ambiguity and potential errors in various downstream applications. The interconversion formulas are similar to those for spherical particles (HT74), but involve coefficient α (Table 1), which is a function of geometric parameters of nonspherical particles such as the degree of effective sphericity Ψ. Furthermore, using the HT74 definition induces a systematic bias in calculating the effective radius of nonspherical particles whose size is defined with size descriptors other than r_{e} (Fig. 1).

In addition, a size descriptor r_{e} can achieve optically quasi-equivalent particle sizes among different nonspherical particles that have consistent Q_{ext} and SSA. The physical background of the optically quasi-equivalent size of arbitrary nonspherical particles is suggested with the modified ADT (Xu et al., 2003; Yang et al., 2004).

Furthermore, we explored nonspherical particle models that achieve optical quasi-equivalence using the roughened hexagonal ice models in the geometric optics regime. The single-scattering properties of three roughened ice crystal models are most consistent for degrees of surface roughness up to 0.15 and fairly consistent for severely roughened cases, with the exception of the quasi-forward phase function. This implies that it is possible to mimic the single-scattering properties of a geometrically complex particle with a simple geometric particle model.

The present findings suggest that Earth-atmosphere system models, cloud–aerosol remote sensing, and analyses of *in-situ* measured atmospheric particles can be further improved by rigorously incorporating nonspherical particle effects, as partly demonstrated in Sections 4e–f. For Earth-system model simulations, the analytical PSD interconversion of nonspherical particles gives exact physical variables required in different modules. For example, an aerosol PSD in terms of volume predicted from a two-moment bulk microphysics model can be easily converted into the number concentration in various particle size ranges without error, which is important to predict the ice nucleating particle concentration (e.g., DeMott et al., 2010). PSDs can also be converted into the extinction coefficient for radiative transfer calculations. For the analyses of *in-situ* measured PSDs, nonspherical particle effects can be incorporated to obtain a unified PSD by combining PSDs measured with different instruments that detect particle sizes based on different size descriptors (e.g., Knopf et al., 2021).

PSDs and associated quantities obtained/computed among Earth system models, remote sensing techniques, and *in-situ* measurements can be made comparable through interconversions that consider nonspherical particle characteristics. This is important for validating numerical models or remotely sensed atmospheric particle properties using *in-situ* observations. Furthermore, the optically quasi-equivalent size of a nonspherical particle suggests that the effective radius should be chosen as a retrieval parameter of particle size rather than other size-representing variables (such as a median radius $\hat{r}_{\mathrm{N}}$) for the remote sensing of atmospheric nonspherical PSDs. This is particularly important if the retrieval variables include some particle shape characteristics (e.g., Herman et al. 2005; Lyapustin et al., 2011a, 2011b) due to the orthogonality of the sensitivity to the particle size and shape variables.

Accepted for publication in *Journal of the Atmospheric Sciences.* DOI 10.1175/JAS-D-22-0086.1.

Thus, the generalization of the PSD interconversions for nonspherical particles shall eliminate the uncertainties associated with nonspherical particle characteristics in many applications involving atmospheric particles. Incorporating this PSD interconversion can be done with little effort, as coefficient α_{pq} primarily governs the interconversions, and the coefficients for the interconversion are listed completely in Tables 2-3.

Acknowledgments.

This research was supported by NOAA Grant NA20NES4400007 and partly by the endowment funds related to the David Bullock Harris Chair in Geosciences at the College of Geosciences, Texas A&M University (grant number 02-512231-0001). We thank James J. Coy Jr. for a preliminary numerical experiment in Section 5d. The numerical computations were conducted with high-performance computing resources provided by Texas A&M University (https://hprc.tamu.edu).

Data Availability Statement.

The data used in this study are generated from mathematical formulas that are thoroughly described in the paper and are implemented into Generalized Nonspherical Particle Size Distribution Package (GeNPSD.pack) that will be available through GitHub after the acceptance of this manuscript.

REFERENCES

Ahmad, Z., B. A. Franz, C. R. McClain, E. J. Kwiatkowska, J. Werdell, E. P. Shettle, and B. N. Holben, 2010: New aerosol models for the retrieval of aerosol optical thickness and normalized water-leaving radiances from the SeaWiFS and MODIS sensors over coastal regions and open oceans. *Appl. Opt.,* **49,** 5545–5560, doi:10.1364/AO.49.005545.

Bi, L., P. Yang, G. W. Kattawar, and M. I. Mishchenko, 2013: Efficient implementation of the invariant imbedding T-matrix method and the separation of variables method applied to large nonspherical inhomogeneous particles. *J. Quant. Spectrosc. Radiat. Transfer,* **116,** 169-183.

Bi, L., and G. Gouesbet, 2022: Debye-series expansion of T-matrix for light scattering by nonspherical particles computed from Riccati-differential equations. *Opt. Express*, **30,** 29796–29810, doi:10.1364/OE.465772.

Bi, L., F. Xu, and G. Gouesbet, 2018: Depolarization of nearly spherical particles: The Debye series approach. *Physical Review A*, **98**(5), 053809.

Blanco, S., and R. Fournier, 2003: An invariance property of diffusive random walks. *EPL (Europhysics Letters)*, **61**(2), 168.

Chylék, P. and G. Videen, 1994: Longwave radiative properties of poly-dispersed hexagonal ice crystals. *J. Atmos. Sci.,* **51,** 175–190.

Cox, C., and W. Munk, 1954: Measurement of the roughness of the sea surface from photographs of the sun's glitter. *J. Opt. Soc. Am.*, **44**(11), 838-850.

Davy, M., M. Kühmayer, S. Gigan, and S. Rotter, 2021: Mean path length invariance in wave-scattering beyond the diffusive regime. *Comm. Phys.*, **4**(1), 1-7.

DeMott, P. J., and Coauthors 2010: Predicting global atmospheric ice nuclei distributions and their impacts on climate. *Proc. Nat. Acad. Sci.,* **107,** 11217-11222.

Dubovik, O., and Coauthors, 2006: Application of spheroid models to account for aerosol particle nonsphericity in remote sensing of desert dust, *J. Geophys. Res.*, **111,** D11208, doi:10.1029/2005JD006619.

Ebert, E. E., and J. A. Curry, 1992: A parameterization of ice cloud optical properties for climate models. *J. Geophys. Res.,* **97,** 3831–3836.

Foot, J. S., 1988: Some observations of the optical properties of clouds. Part II: Cirrus. *Quart. J. Roy. Meteor. Soc.,* **114,** 145– 164.

Fu, Q., 1996: An accurate parameterization of the solar radiative properties of cirrus clouds for climate models. *J. Climate,* **9,** 2058–2082.

Grenfell, T. C., and S. G. Warren, 1999: Representation of a non-spherical ice particle by a collection of independent spheres for scattering and absorption of radiation. *J. Geophys. Res.,* **104,** 31697–31709, https://doi.org/10.1029/1999JD900496.

Ham, S.-H., S. Kato, and F. G., Rose, 2017: Examining impacts of mass-diameter (m-D) and area-diameter (A-D) relationships of ice particles on retrievals of effective radius and ice water content from radar and lidar measurements, *J. Geophys. Res. Atmos.,* **122,** 3396–3420, doi:10.1002/2016JD025672.

Hansen, J., and L. Travis, 1974: Light scattering in planetary atmospheres. *Space Sci. Rev.,* **16,** 527–610.

Herman, M., J.-L. Deuzé, A. Marchand, B. Roger, and P. Lallart, 2005: Aerosol remote sensing from POLDER/ADEOS over the ocean: Improved retrieval using a nonspherical particle model, *J. Geophys. Res.*, **110,** D10S02, doi:10.1029/2004JD004798.

Heymsfield, A. J., and L. M. Miloshevich, 2003: Parameterizations for the cross-sectional area and extinction of cirrus and stratiform ice cloud particles. *J. Atmos. Sci.*, **60,** 936–956.

——, A. Bansemer, C. Schmitt, C. Twohy, and M. R. Poellot, 2004: Effective ice particle densities derived from aircraft data. *J. Atmos. Sci.*, **61,** 982–1003.

——., C. Schmitt, and A. Bansemer, 2013: Ice cloud particle size distributions and pressure-dependent terminal velocities from in situ observations at temperatures from 0 to −86°C. *J. Atmos. Sci.*, **70**(12), 4123-4154.

Hinds, W. C. 1999: *Aerosol Technology: Properties, Behavior, and Measurement of Airborne Particles, 2nd Edition*. Wiley, 504 pp. pp.

Hioki, S., P. Yang, B. A. Baum, S. Platnick, K. G. Meyer, M. D. King, and J. Riedi 2016: Degree of ice particle surface roughness inferred from polarimetric observations, *Atmos. Chem. Phys*, **16**(12), 7545–7558.

Hioki, S. 2018: *Characterizing Ice Cloud Particle Shape and Surface Roughness from Polarimetric Satellite Observations* (Doctoral dissertation).

Johnson B. R., 1988: Invariant imbedding T-matrix approach to electromagnetic scattering. *Appl. Opt.*, **27,** 4861–4873.

Junge, C., 1955: The size distribution and aging of natural aerosols as determined from electrical and optical data on the atmosphere. *J. Meteor.*, **12,** 13–25, doi:10.1175/1520-0469(1955)012,0013:TSDAAO.2.0.CO;2.

Knopf, D. A., and Coauthors 2021: Aerosol–ice formation closure: A southern Great Plains field campaign. *Bull. Amer. Meteor. Soc.*, **102**(10), E1952-E1971.

Korolev, A. V., and G. Isaac, 2003: Roundness and aspect ratio of particles in ice clouds. *J. Atmos. Sci.,* **60,** 1795–1808, doi:10.1175/1520-0469(2003)060,1795:RAAROP.2.0.CO;2.

Lawson, R. P., and Coauthors, 2019: A review of ice particle shapes in cirrus formed in situ and in anvils. *J. Geophys. Res. Atmos.,* **124,** 10049–10090, https://doi.org/10.1029/2018JD030122.

Lee, J., N. C. Hsu, A. M. Sayer, C. Bettenhausen, and P. Yang, 2017: AERONET-based nonspherical dust optical models and effects on the VIIRS deep blue/SOAR over water aerosol product, *J. Geophys. Res.-Atmos.,* **122,** 10441–10458.

Liou, K. N., 1992: *Radiation and Cloud Processes in the Atmosphere.* Oxford University Press, 487 pp.

Liu, C., Panetta, R. L., and Yang, P. 2013: The effects of surface roughness on the scattering properties of hexagonal columns with sizes from the Rayleigh to the geometric optics regimes, *J. Quant. Spectrosc. Radiat. Transfer,* **129,** 169–185, https://doi.org/10.1016/j.jqsrt.2013.06.011.

Liu, C., R. L. Panetta, and P. Yang, 2014: The effective equivalence of geometric irregularity and surface roughness in determining particle single-scattering properties. *Opt. Express,* **22,** 23620–23627, doi:10.1364/OE.22.023620.

Lindqvist, H., O. Jokinen, K. Kandler, D. Scheuvens, and T. Nousiainen, 2014: Single scattering by realistic, inhomogeneous mineral dust particles with stereogrammetric shapes, *Atmos. Chem. Phys.,* **14,** 143–157, https://doi.org/10.5194/acp-14-143-2014.

Lyapustin, A., J. Martonchik, Y. Wang, I. Laszlo, and S. Korkin, 2011a: Multiangle implementation of atmospheric correction (MAIAC): 1. Radiative transfer basis and look-up tables. *J. Geophys. Res.,* **116,** D03210, https://doi.org/10.1029/2010JD014985.

——, Y. Wang, I. Laszlo, R. Kahn, S. Korkin, L. Remer, R. Levy, and J. S. Reid, 2011b: Multiangle implementation of atmospheric correction (MAIAC): 2. Aerosol algorithm. *J. Geophys. Res.,* **116,** D03211, https://doi.org/10.1029/2010JD014986.

Magee, N., and Coauthors, 2021: Captured cirrus ice particles in high definition, *Atmos. Chem. Phys.*, **21,** 7171–7185, https://doi.org/10.5194/acp-21-7171-2021.

Miles, N. L., J. Verlinde, and E. E. Clothiaux, 2000: Cloud droplet size distributions in low- level stratiform clouds. *J. Atmos. Sci.*, **57(2),** 295–311. https://doi.org/10.1175/1520- 0469(2000)057<0295:CDSDIL>2.0.CO;2

Nakajima, T., G. Tonna, R. Rao, P. Boi, Y. Kaufman, and B. Holben, 1996: Use of sky brightness measurements from ground for remote sensing of particulate polydispersions. *Appl. Opt.*, **35**(15), 2672-2686.

Ono, A., 1970: Growth mode of ice crystals in natural clouds. *J. Atmos. Sci.*, **27,** 649–658.

Petty, G. W. and Huang, W. 2010: Microwave backscatter and extinction by soft ice spheres and complex snow aggregates, *J. Atmos. Sci.,* **67,** 769–787.

Petty, G. W. and Huang, W. 2011: The modified gamma size distribution applied to inhomogeneous and nonspherical particles: Key relationships and conversions, *J. Atmos. Sci.,* **68,** 1460–1473.

Reid, E. A., and Coauthors, 2003a: Characterization of African dust transported to Puerto Rico by individual particle and size segregated bulk analysis. *J. Geophys. Res.*, **108(D19),** 8591. https://doi.org/10.1029/ 2002JD002935.

Reid, J. S., and Coauthors, 2003b: Comparison of size and morphological measurements of coarse mode dust particles from Africa. *J. Geophys. Res.*, **108**(D19), 8593. https://doi.org/10.1029/ 2002JD002485a

Platnick, S. and Coauthors, 2017: The MODIS cloud optical and microphysical products: Collection 6 updates and examples from Terra and Aqua. *IEEE Trans. Geosci. Remote Sens.,* **55,** 502–525, https://doi.org/10.1109/TGRS.2016.2610522.

Saito, M. and P. Yang, 2021: Advanced bulk optical models linking the backscattering and microphysical properties of mineral dust aerosol, *Geophys. Res. Lett.,* **48,** e2021GL095121, https://doi.org/10.1029/2021GL095121.

Saito, M., P. Yang, J. Ding, and X. Liu, 2021: A comprehensive database of the optical properties of irregular aerosol particles for radiative transfer simulations. *J. Atmos. Sci.*, **78,** 2089–2111, https://doi.org/10.1175/JAS-D-20-0338.1

Schladitz, A., and Coauthors, 2009: In situ measurements of optical properties at Tinfou (Morocco) during the Saharan Mineral Dust Experiment SAMUM 2006, *Tellus,* **61B,** 64-78.

Takano, Y., and K. N. Liou, 1989: Solar radiative transfer in cirrus clouds. Part I: Single-scattering and optical properties of hexagonal ice crystals, *J. Atmos. Sci.,* **46(1),** 3-19.

Um, J., G. M. McFarquhar, Y. P. Hong, S.-S. Lee, C. H. Jung, R. P. Lawson, and Q. Mo, 2015: Dimensions and aspect ratios of natural ice crystals. *Atmos. Chem. Phys.*, **15,** 3933–3956, doi:10.5194/ acp-15-3933-2015.

van de Hulst, H. C., 1957: *Light Scattering by Small Particles.* John Wiley and Sons, 470 pp.

van Diedenhoven, B., B. Cairns, I. Geogdzhayev, A. Fridlind, A. Ackerman, P. Yang, and B. Baum, 2012: Remote sensing of ice crystal asymmetry parameter using multi-directional polarization measurements–Part 1: Methodology and evaluation with simulated measurements, *Atmos. Meas. Tech.*, **5,** 2361–2374.

Volten, H., O. Muñoz, E. Rol, J. F. de Haan, W. Vassen, and J. W. Hovenier, 2001: Scattering matrices of mineral aerosol particles at 441.6 nm and 632.8 nm. *J. Geophys. Res.*, **106,** 17375–17401. https://doi.org/10.1029/2001JD900068

Vouk, V., 1948: Projected area of convex bodies. *Nature*, **162,** 330-331.

Wadell, H., 1935: Volume, shape and roundness of quartz particles. *J. Geology*. **43**, 250–280.

Wyser, K., 1998: The effective radius in ice clouds. *J. Clim.,* **11,** 1793–1802.

Wyser, K., and P. Yang, 1998: Average ice crystal size and bulk shortwave single scattering properties of cirrus clouds, *Atmos. Res.*, **49,** 315-335.

Xu, M, M. Lax, and R. R. Alfano, 2003: Light anomalous diffraction using geometrical path statistics of rays and Gaussian ray approximation. *Opt. Lett.* **28,** 179–181.

Xu, F., J. A. Lock, and C. Tropea, 2010: Debye series for light scattering by a spheroid. *JOSA A*, **27**(4), 671-686.

Yang, P., and K. N. Liou, 1996: Geometric-optics-integral-equation method for light scattering by nonspherical ice crystals, *Appl. Opt.*, **35,** 6568–6584.

Yang, P. and K. N. Liou, 1998: Single-scattering properties of complex ice crystals in terrestrial atmosphere, *Contr. Atmos. Phys.*, **71 (2),** 223–248.

Yang, P., B. A. Baum, A. J. Heymsfield, Y. X. Hu, H. L. Huang, S. C. Tsay, and S. Ackerman, 2003: Single-scattering properties of droxtals. *J. Quant. Spectrosc. Radiat. Transfer*, **79,** 1159-1169

Yang, P., Z. Zhang, B. A. Baum, H.-L. Huang, and Y. Hu, 2004: A new look at anomalous diffraction theory (ADT): Algorithm in cumulative projected-area distribution domain and modified ADT. *J. Quant. Spectrosc. Radiat. Transfer,* **89 (1–4),** 421–442, doi:10.1016/j.jqsrt.2004.05.038.

Yang, P., L. Bi, B. A. Baum, K. N., Liou, G. L., Kattawar, M. I., Mishchenko, and B. Cole, 2013: Spectrally consistent scattering, absorption, and polarization properties of atmospheric ice crystals at wavelengths from 0.2 to 100 μm, *J. Atmos. Sci.*, **70,** 330–347.